Document Number**:** H2020-ICT-52/RISE-6G/D6.2

Project Name:
Reconfigurable **I**ntelligent **S**ustainable **E**nvironments for **6G** Wireless Networks (RISE-6G)

Deliverable D6.2

Sustainable RIS solutions design for EE, EMFEU and SSE (Intermediary Specifications)

Date of delivery:	30/06/2022	Version:	FINAL
Start date of Project:	01/01/2021	Duration:	36 months

Deliverable D6.2

Sustainable RIS solutions design for EE, EMFEU and SSE (Intermediary Specifications)

Project Number:	101017011
Project Name:	**R**econfigurable **I**ntelligent **S**ustainable **E**nvironments for **6G** Wireless Networks

Document Number:	H2020-ICT-52/RISE-6G/D6.2
Document Title:	Sustainable RIS solutions design for EE, EMFEU and SSE (Intermediary Specifications)
Editor(s):	D.-T. Phan Huy (ORA)
Authors:	N. Awarkeh, R. Ibrahim, D.-T. Phan Huy, P. Ratajczak, Y. Yu (ORA) M. Di Renzo (CNRS) G. Gradoni, G. Tanner (UNOT) L. Bastianelli, E. Colella, V. Mariani Primiani (CNIT) E. Calvanese Strinati, F.-E. Fairod (CEA) H. Guo, T. Svensson (CHAL) R. Kotaba, P. Popovski (AAU) G. C. Alexandropoulos, K. D. Katsanos (NKUA).
Dissemination Level:	PU
Contractual Date of Delivery:	30/06/2022
Security:	Public
Status:	FINAL
Version:	FINAL
File Name:	RISE-6G_WP6_D6.2_Final.docx

Abstract

In this deliverable, we summarize the intermediate results of Task 6.2 on Sustainable RIS Solutions Design for EE, EMFEU and SSE and Task 6.3 on assessment methods of EE, EMFEU and SSE Improvements.
We present eight solutions and innovations to boost the EE, EMFEU or SSE metrics and three new models to assess these metrics. Final results will be provided in the upcoming deliverable D6.3.

Keywords

Beyond-5G; 6G; RIS; Secrecy, Security; EMF exposure; Energy-Efficiency

Contents

List of Figures

List of Tables

List of Acronyms

3D	Three-Dimension
5G	Fifth Generation
6G	Sixth Generation
AO	Alternating Optimization
AP	Access Point
BA	Binary Amplitude
BC	Boundary Conditions
BF	Beamforming
BOA	Blue Optimization Algorithm
BRT	Battery Recharging Time
BS	Base Station
CPU	Central Processing Unit
CRKG	Channel Reciprocity-based Key Generation
CSI	Channel State Information
DFT	Discrete Fourier Transform
DL	Downlink
DMA	Dynamic Metasurface Antenna
E2E	End-To-End
EE	Energy-Efficiency
EMF	Electromagnetic-Field
EMFE	Electromagnetic-Field Exposure
EMFEU	EMFE Utility
ER	Energy Receivers
FDTD	Frequency Discrete Time Discrete
GSTC	Generalized Sheet Transition Conditions
ICNIRP	International Commission on Non-Ionizing Radiation Protection
I	Intended
I-UE	Intended User Equipment
IU	Intended User
LP	Lorentzian-constrained Phase
MAC	Medium Access Control
MEC	Multi-access Edge Computing
MEH	Mobile Edge Host
MIMO	Multiple Input Multiple Output
MMIMO	Massive Multiple-Input Multiple-Output
mmWave	Millimeter Wave
MRT	Maximum Ratio Transmission
NIU	Non Intended User
NI	Non Intended
NI-UE	Non Intended User Equipment
OFDM	Orthogonal Frequency Division Multiplexing

PHY	Physical
RC	Reverberating Chamber
RFEH	Radio Frequency energy harvesting
RIS	Reconfigurable Intelligent Surface
SAR	Specific Absorption Rate
SDR-SCA	Semi-definite Relaxation-Successive Convex Approximation
SNR	Signal-to-Noise Ratio
SSE	Secrecy Spectral Efficiency
TDD	Time Division Duplex
UE	User Equipment
UL	Uplink
UT	User Terminal
WP	Workpackage
WPT	Wireless Power Transfer
ZF	Zero-Forcing

1 Introduction

RISE-6G is a 5G-PPP project funded by the European Commission under the H2020 framework. The project's vision hinges on the latest advances on reconfigurable intelligent surfaces (RISs) technology for radio wave propagation control, with the aim of improving this technology, and conceiving sustainable, programmable, and goal-oriented wireless environments. The main objectives of RISE-6G are: (i) the definition of novel architectures and control strategies incorporating multiple RISs; (ii) the study of the fundamental limits of the RIS technology based on realistic and validated radio wave propagation models; (iii) the design, by three different workpackages (WPs), of algorithmic frameworks based on RIS-empowered smart wireless environments providing enhanced connectivity and reliability (WP4), enhanced localisation accuracy (WP5), and enhanced sustainability and security (WP6); (iv) the prototyping of the proposed innovation via two complementary trials with verticals. Deployment scenarios and use cases are defined by WP2.

Within RISE-6G, WP6 proposes innovative Physical (PHY) layer and Medium Access Control (MAC) layer technical enablers to improve the sustainability and security of wireless networks. More precisely, WP6 proposes solutions to boost the performance of wireless networks in terms of energy-efficiency (EE), electromagnetic-field (EMF) exposure (EMFE) utility (EMFEU), and secrecy spectral efficiency (SSE) metrics, as defined in Deliverable D2.4. WP6 aims at improving these metrics focusing on spatially localised areas. Such performance "boosted areas" have been defined in Deliverable D2.3 and identified for various deployment scenarios and use cases listed in the same deliverable. It is expected that the EE, EMFEU, and SSE metrics require specific and novel network architectures & deployment strategies with RISs, as well as novel assessment methods of their consideration.

D6.1 provides the intermediate results from WP6, on network architectures and deployment strategies with RIS to boost the EMFEU and SSE metrics defined in Deliverable D2.4, for the use cases listed in D2.3. The deliverable lists several architectural options, RIS control strategies, as well as related data flows and control signalling, all derived from various technical contributions and innovations proposed within WP6.

To summarize, the following concepts apply to both EMFEU- and SSE-boosted networks and guide the way we design our solutions:

- Radio waves are *desirable* at the position of an *intended* entity (device, user, person, or object), because this entity is receiving data from the network or is sensed by the network.
- Radio waves are *undesirable* at the position of a *non-intended* entity (device, user, person, or object) which can be either an *exposed* entity for which EMFE is undesirable, or an *eavesdropper* towards whom signal reception is undesirable.
- A *non-intended* entity (device, user, person, or object) can be either *not helping* or *helping* the network to boost the EMFEU or the SSE.
- In the case of EMFEU, the *helping non-intended* entity can help *intentionally* by participating to the protocol reducing the EMFE.
- In the case of SSE, the *non-intended* entity is always helping in a *non-intentional* manner. The network simply exploits an existing connection and the corresponding control information exchanged between the *non-intended* entity and itself.

Also, in this deliverable, the impact of the designed schemes on the EE metric is discussed.

Most proposed schemes rely on hybrid RISs that can switch between different modes, including at least a reflecting and a receiving mode, and for some schemes, a transmitting mode as well as a transparent mode.

1.1 Deliverable objectives & methodology

This document provides the intermediate results from WP6, on Task 6.2 and 6.3.

In Task 6.2, we design innovations in PHY-MAC layers to reach the target objectives in the target "EE/EMFEU/SSE boosted areas". We also propose innovative schemes to optimize the trade-off between EE and EMFEU or the trade-off between EE and SSE, in the particular cases where EMFEU and/or SSE is improved at the expense of EE. We recall that the EE, EMFEU, SSE metrics and the boosted areas have been defined in D2.3 (deployment scenarios and use cases) and D2.4 (metrics), and D6.1 (initial views on architecture and control signalling aspects).

The main objective of Task 6.3 is to assess the improvement in terms of EE, EMFEU and SSE brought by RISE network with architectures identified in Task 6.1 (see Deliverable D6.1) and innovations from Task 6.2 (See Section 2) based on advanced realistic models provided by WP3. To do so, we exploit our measurements of actual RIS (built by the project) and a true 5G BS in a Reverberating Chamber (RC), advanced modelling tools developed in WP3, FDTD or Finite Elements simulations, and new mathematical frameworks, exploiting a Random Coupling Model (RCM).

Each of the proposed schemes aimed at boosting EMFEU, is **based on general principles explained in D6.1 and recalled hereafter.**

First of all, the control of EMFE towards humans, other living beings as well as certain objects that should have a limited EMFE needs to be reflected in specific protocol operations that take place in a RIS-aided communication system. In general, the communication system needs to differentiate between spatial points where the radiation is *desirable* and *undesirable*. The spatial points with *desirable* radiation are the ones occupied by an *intended* entity: an *intended* receiver (for instance held by an *intended user* of the communication link) that will receive the radio waves, an *intended* object or person that needs to be illuminated by radio waves in order to be sensed by the network. Hence, radio waves are *desirable* at the position of *intended* receivers, *intended* users and *intended* sensed humans or objects. At the spatial points with *undesirable* radiation, the EMFE needs to be kept below a certain value. The International Commission on Non-Ionizing Radiation Protection (ICNIRP) (D6.1) provides recommendation regarding such threshold, based on the analysis of scientific studies. However, it can happen that some countries or cities adopt more constraining limits than the ICNIRP guidelines [GSMA]. Also, some use cases presented in D2.3 and D2.4 propose to provide "EMFEU boosted areas" as a service, for instance, in a Train Station. Therefore, the threshold can be set arbitrarily low, either by a city, a country, or a building owner. Note that according to the local regulation, the threshold usually must be ensured in a statistical sense (for instance on average and during a given pre-defined period) (D6.1). The spatial points with *undesirable* radiation are the ones occupied by a *non-intended exposed* entity: a *non-intended exposed* user (a user of the communication network having subscribed to a low EMFE service), a *non-intended exposed* person or object. There are two main ways in which the communication system can detect and control *undesirable* EMFE at the *non-intended exposed* entity (user, person, or object), depending on the level of participation of *non-intended exposed* entity to the communication system protocol:

- The *non-intended exposed* entity is *not helping:* In this case the *non-intended* entity does not provide information about its positioning or status of EMFE, such that the communication system needs to infer it based on its own sensing capabilities, or by interfacing to application programming interface (APIs) and systems that can provide such information. For example, there could be a different system that measures room occupancy and based on that information the communication system can adjust the calculation of the induced EMFE.

- The *non-intended exposed* entity is *intentionally helping:* This is the case in which the *non-intended exposed* entity explicitly provides information to the communication system to assist the control of EMFE. For example, the device associated with a *non-intended exposed* user can use some of its signalling messages to indicate the level of EMFE or, simply, to make itself known to the communication system in order to force it to limit the EMFE at that spatial location. Such active methods for EMFE control may require dedicated protocol messages that can initiate certain action, such as change of the RIS pattern or decrease of the transmit power.
- Note that there could also be a non-intended exposed user helping non-intentionally (similarly as eavesdropper, i.e. limited to the control info).

Our proposed design solutions for boosted SSE are based upon the same general principles as for EMFEU boosting. Indeed, an *eavesdropper* is similar to a *non-intended exposed* user. Again, there are two main ways in which the communication system can detect and control *undesirable* signal at the *eavesdropper*, depending on the level of participation of the *eavesdropper* to the communication system protocol:

- The *eavesdropper* is *not helping:* In this case the *eavesdropper* does not provide information about its positioning or status of received signal, such that, as for the exposed user, the communication system needs to infer it based on its own sensing capabilities. In the worst case, i.e., without any knowledge regarding the eavesdropper, the network would simply try to reduce the level of signal in general; note that such eavesdropper is complex.
- The *eavesdropper* is *non-intentionally helping:* This is the case in which the *eavesdropper* is itself a User Equipment (UE), such as a smartphone, connected to the communication network. In this case, like any UE connected to the network, the eavesdropper exchanges data, control signals and pilots with the network. However, contrary to a normal UE, the eavesdropper tries to demodulate messages sent over radio resources allocated to another user equipment. To avoid such type of eavesdropping, the network could use pilot, control and data signals circulating between itself and the eavesdropper. In this case, the eavesdropper *non-intentionally helps* the network to improve its SSE; note that such eavesdropper is less complex as it is very close to a standard commercial device.

Figure 1-1 below illustrates the aforementioned concepts with one example where a RISE network emits radio waves with the Intended User as a target, in the presence of four Non-Intended entities:

1. A *Non-Intended User* who uses his/her UE (connected to the network) to *eavesdrop*; the network uses the connection with the *eavesdropper* to avoid eavesdropping, and thus the eavesdropper *unintentionally helps* the network.
2. A *Non-Intended User* who is *exposed* to the radio waves emitted by the RISE network, and who uses his/her UE (connected to the network) to *help intentionally*, the network to reduce his/her exposition.
3. A *Non-Intended* person, who is *exposed* to the radio waves emitted by the RISE network but is *not helping* the network to reduce his/her exposition.
4. A *Non-Intended* person, who uses a device (which is not connected to the network) to *eavesdrop*, *without helping* the network to prevent him/her from eavesdropping.

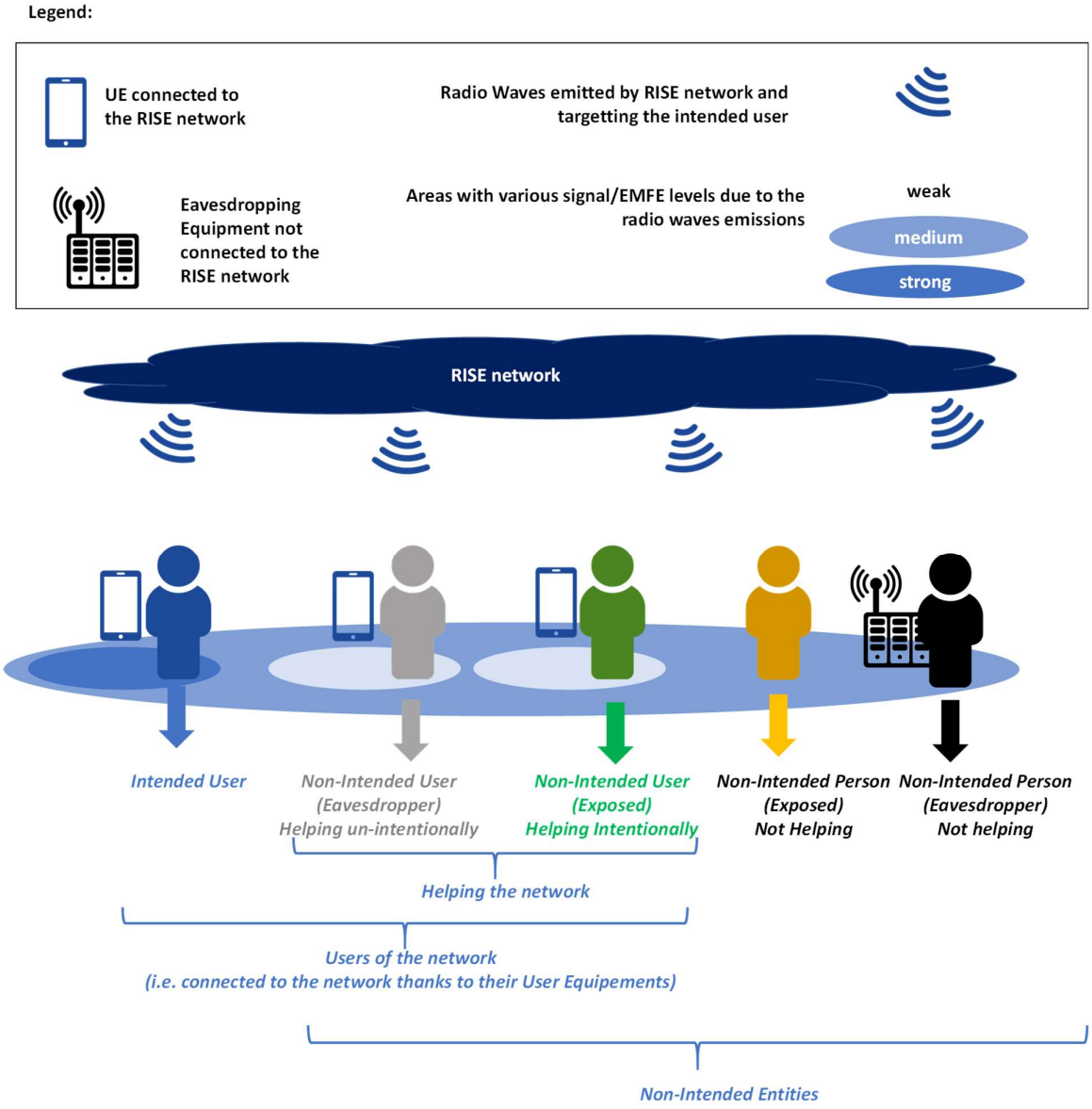

Figure 1-1 Example where the RISE network emits radio waves with the Intended User as a target, in the presence of four different types of Non-Intended entities (Figure extracted from D6.1).

Finally, we recall that there are two types of EMFE (as defined in D2.4):

- Inter-EMFE: exposure of a Non Intended User to waves, in uplink (UL) or downlink (DL) transporting data for another Intended User.
- Self-EMFE: exposure of a User to waves (in UL or DL) transporting his/her own data (in this case the user is at the same time Intended and Non Intended).

1.2 Deliverable structure

The deliverable is organised as follows.

In Section 2, for each of the various PHY-MAC solutions or innovations proposed by WP6, Task 6.2, to boost SSE or EMFEU, a brief description is provided. Table 1-1 lists the proposed solutions and the metric on which they are focused.

Section	Metric	Proposed Innovation
2.1	Inter-EMFEU & EE	Inter-EMFE aware beamforming (BF) assisted by RIS: Directional Spreading, Truncation and Boosting
2.2	Inter-EMFEU	Inter-EMFE aware BF assisted by RIS: Using an Angularly Equalized Virtual Propagation Channel
2.3	Inter-EMFEU	Inter-EMFE aware BF assisted by RIS: the Multi-User Multiple Input Multiple Output (MU-MIMO) case
2.4	Inter-EMFEU	The RIS opportunity to reduce EMFE, using optimization tools
2.5	EE & Self-EMFEU	Energy Efficiency Optimization of Reconfigurable Intelligent Surfaces with self-EMFE Constraints
2.6	Inter-EMFEU & EE	RIS Solution for enhanced EE and EMFEU
2.7	EE	Energy efficiency maximization of Massive MIMO (MMIMO) communications with dynamic metasurface antennas
2.8	SSE	On Maximizing the Sum Secret Key Rate for Reconfigurable Intelligent Surface-Assisted Multiuser Systems

Table 1-1 Task 6.2 solutions or innovations, and metric on which they are focused

Section 3 provides progress status on the following new models, which were developed within Task 6.3:

- 3.1: Battery recharging time models for reconfigurable intelligent surfaces-assisted wireless power transfer systems
- 3.2: Development of modeling tools by FDTD methods, and integration with framework provided by WP3 .
- 3.3: Power balance model for RIS-assisted RC (method for estimating the average EMFEU in complex scattering environments).

2 Sustainable RIS Solutions Design for EE, EMFEU and SSE

In this section, we summarize the work performed within Task 6.2. For each of the various contributions, the following brief description is provided:

- Objective.
- System model.
- Initial performance results (if available).
- Conclusion.

Note that for more mature schemes, the detailed description of the proposed schemes and their performance is available in submitted/accepted papers. For other schemes, at an earlier stage of study, only initial views on expected performance are provided. For those latter schemes, finalized results will be provided in the upcoming deliverable D6.3.

Note that, although the proposed schemes have been identified to have an impact on the metrics of EE, EMFEU and SSE as defined in D2.4, their descriptions, in the current deliverable, do not necessarily use exactly the same metrics. The link between the metrics used in the descriptions and the D2.4 metrics will be clarified in the upcoming D6.3 deliverable.

2.1 Inter-EMFE aware BF assisted by RIS: Directional Spreading, Truncation and Boosting

The current sub-section summarizes a study that is detailed in [APV21] and [APV+22-1].

2.1.1 Introduction

MMIMO systems and adaptive BF enable mobile networks to deliver high throughput [MHM+18] [R+13]. As an example, a Base Station (BS) transmitting with its maximum power maximizes the received power and the delivered data rate at the target UE thanks to Maximum Ratio Transmission (MRT) BF scheme [L99] and an MMIMO antenna [VGT14]. Additionally, the regulation specifies a maximum EMFE threshold. This threshold must not be exceeded, beyond a limit region (typically a circle in environment without obstacles close to the BS), *with a given probability or on average, during a time window*, depending on the regulation. However, when the BS must serve the same user for a long period, in some cases, MMIMO and MRT BF could generate an over-exposed area exceeding the limit circle, in some directions, and cannot be used or deployed as such [TFC+17] [DTT16] [XZY+19] [PCE+18] [C+19] [CEA21]. As illustrated in Figure 2-1-a), these strong directions correspond to prime propagation paths between the antenna and the receiver. Also, we foresee that in the future, even arbitrarily larger limit circles and more stringent thresholds could be requested in the future by some cities. One simple solution to comply with the EMFE constraint consists in using a reduced transmit power at the BS (whilst keeping using MRT BF) that ensures that the entire over-exposed area gets inside the circle, even in its strongest directions, and for a long period. Unfortunately, as illustrated in Figure 2-1-b), such a Reduced MRT BF scheme reduces the received power at the target UE and degrades the received QoS. To overcome this drawback, we propose a first new EMF aware BF scheme, named Truncated MRT. It truncates the MRT BF radiation pattern, only in the directions where the over-exposed area would exceed the limit circle otherwise. The other directions already inside the circle are not impacted by the truncation. Compared to the Reduced MRT BF scheme, the Truncated MRT BF scheme uses a transmit power that is higher and delivers a received power at the target UE that is stronger, whilst remaining compliant with the EMFE constrain. To further improve the performance, we propose a second novel RIS-aided scheme, named Truncated and Boosted MRT BF scheme. As illustrated in Figure 2-1-d), this scheme boosts the remaining directions inside the circle until they meet the circle. Finally, to further enhance the performance of the aforementioned BF schemes, we propose to exploit the nascent concept of smart radio environments for the future 6th generation network (6G), by shaping the propagation environment itself (according to some Channel State Information (CSI)) thanks to RISs [R+19] [BRR+19] [S+21] [IEA+22] [ZR22] [R+21-1]. Note that in [IEA+22] [ZR22], RISs are used to reduce self-EMFE due to the smartphone UL, whereas we use RISs for EMFE reduction in the DL. More precisely, a RIS with continuous (instead of discrete) phase-shifting capability as in [R+21-1] [R+21-2] and sensing capability, first measures the propagation channel between the target UE and itself, and then, self-configures to ‘turn itself electronically’ in the direction of the target UE. Several sensing and self-tuning RISs of such type are deployed in the environment. Hence, without any communication with the RISs, MRT BF, Reduced MRT BF, and Truncated MRT BF schemes (all derived from MRT) naturally spread their radiation patterns in additional directions. As illustrated in Figure 2-1-a), b) and c), these directions are the directions of the RISs.

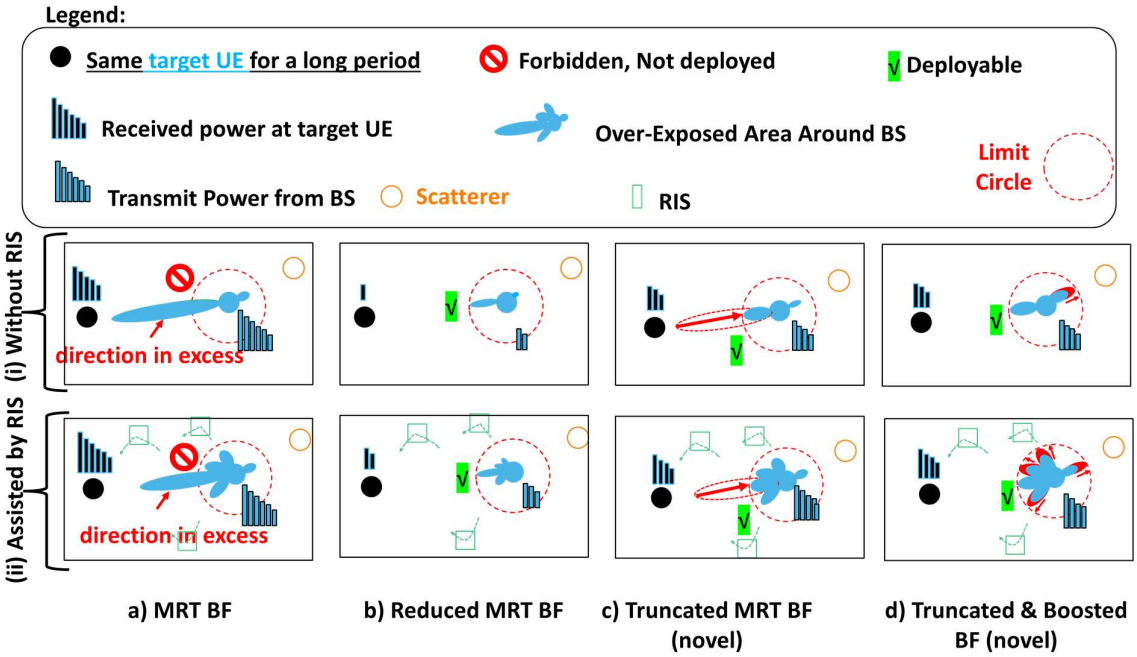

Figure 2-1 Studied BFs and corresponding over-exposed areas, assuming that the same UE is served by the BS for a long period

2.1.2 System Model

In this study, we consider the DL data transmission between a M-MIMO BS equipped with 64 antenna elements and a target UE. The BS is aided by 3 RISs randomly positioned, of 16 elements each. We consider a multipath propagation environment with 3 random scatterers. The propagation channel between the BS, the RIS and the target UE is modelled using the planar wave approximation, as illustrated in Figure 2-2-a). The propagation between the BS and a point Q close to the BS, is modelled using spherical waves, assuming free space propagation. As illustrated in Figure 2-2-b), the following two-step procedure applies:

- during the RIS Self-Configure procedure, the target UE sends pilots, and the RIS estimates the UE-to-RIS channel phases and self-configures its weight to “turn itself electronically” towards the UE.
- During the BS BF procedure, the target UE sends pilots again, and the BS estimate the UE-to-BS channel (under the influence of the RIS) and computes the MRT BF scheme.

The propagation between the BS and any point onto the limit circle is assumed to be perfectly known by the BS (for instance, thanks to previous measurements). Hence, knowing the BF precoder expression, the BS can predict the exposure onto the limit circle.
For reduced BF scheme, the BS uses the MRT BF scheme with a reduced transmit power ensuring that the EMFE target constraint is met onto the limit circle. For the truncated BF scheme, the BS projects the MRT BF scheme onto a codebook of DFT beams to enable a per-beam (and per-direction) control of the radiation pattern of the BF precoder. Then, the BS truncates beams that exceed the limit circle. For the truncated and boosted BF scheme, the BS modifies the truncated BF precoder, by boosting the beams (directions) remaining inside the circle, until they meet the limit circle.

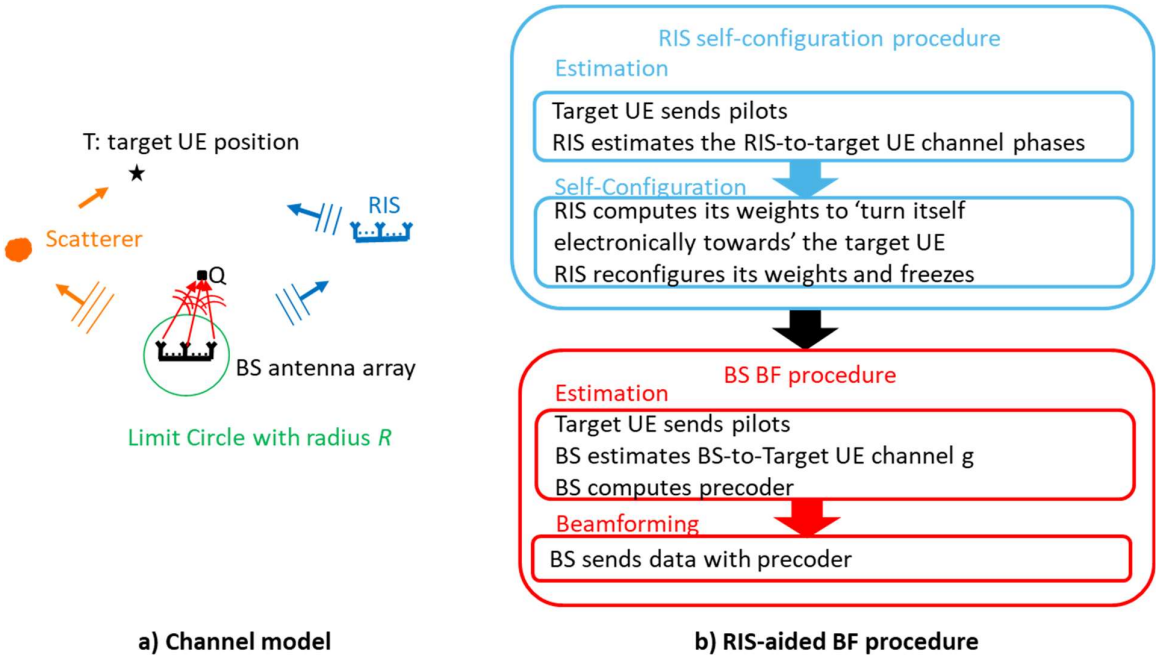

Figure 2-2 System Model.

The channel random parameters are drawn, and for each simulation sample, the following performance metrics are computed:

- The received power at the target UE.
- The BS transmit power.
- The percentage of positions exceeding the EMFE constraint beyond the limit circle (calculated inside a square surrounding the circle).

The mathematical details of the channel model and the procedures and simulation assumptions are provided in [APV21] and [APV+22-1].

2.1.3 Results

Figure 2-3 illustrates statistics of the performance metrics introduced in 2.1.3, over random channels. Figure 2-3-a) illustrates the CDF of the percentage of positions exceeding the EMFE constraint (assuming the same UE is targeted for a long period), beyond the limit circle. Figure 2-3-b) illustrates the CDF of the BS transmit power and Figure 2-3-c) illustrates the CDF of received power at the target UE. Performance with and without RIS assistance is plotted. MRT BF alone is not deployable. Reduced BF is compliant with the EMFE constrains but provides a low received power at the target UE. The Truncated and Boosted BF scheme maximises the received power at the target UE and better matches the constrain. However, it uses a large transmit power at the BS side. The truncated BF scheme alone perfectly matches the constraint and is more energy-efficient. Detailed results and assumptions are available in [APV21] and [APV+22-1].

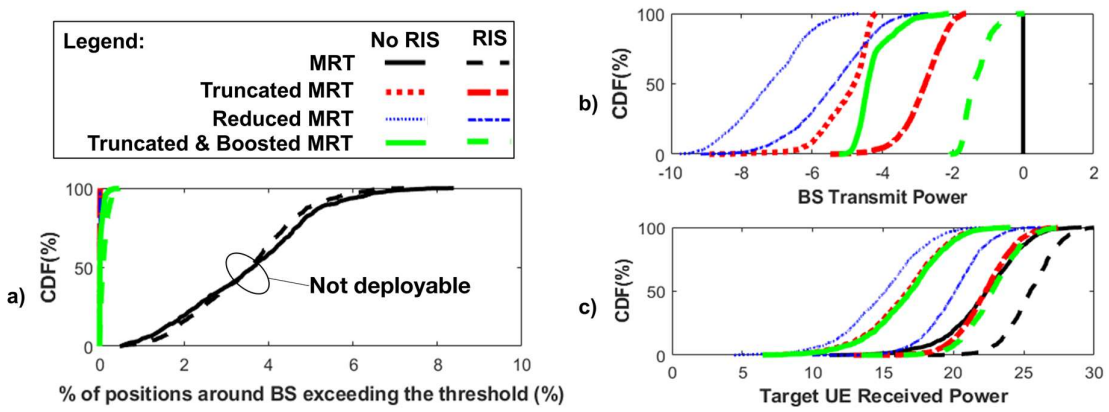

Figure 2-3 System Model CDFs of a) positions around BS (inside a square around the BS) exceeding the threshold b) BS transmit power and c) target UE received, assuming the same UE is targeted for a long period.

2.1.4 Conclusion

In this study, we propose two novel RIS-aided BF schemes called Truncated BF scheme and Truncated and Boosted BF scheme. They are built based on the projection of the MRT BF on the DFT codebook to allow truncation and boosting of individual beams (directions). We compare them to the MRT BF scheme (which is exceeds the EMFE constrain, when the same UE is targeted for a long period) and the Reduced MRT BF scheme (which delivers a poor received power at the target UE). Truncated BF scheme provides a better throughput than Reduced BF scheme, it perfectly matches the EMFE constrain, and it is more energy efficient than Truncated and Boosted BF scheme. Therefore, the Truncated BF scheme boosts the inter-EMFEU and the EE.

2.2 Inter-EMFE aware BF assisted by RIS: Using an Angularly Equalized Virtual Propagation Channel

The current sub-section summarizes a study that is detailed in [APV+22-2].

2.2.1 Introduction

In this study, we address the same problem as already presented in Section 2.1. However, we propose another novel RIS-aided BF scheme, named Equalized BF scheme, exploiting the channel sounding capability of the MMIMO BS [WK14][TP16][W+20] to provide high throughput under EMFE constraint. In this study, instead of the using the CSI of the true channel, to compute the MRT BF precoder, we propose to use the CSI of a virtual propagation. The virtual propagation channel is computed based on a sounding of the true channel. Compared to the true channel, the virtual channel, has the same scatterers, in the same directions. However, the virtual channel, is equalized in the angular domain: the path gain of all scatterers is set to 1. As a consequence, the radiation pattern of the MRT BF will also be equalized in the angular domain. The BS computes the transmit power to ensure that the EMFE constraint is met on the limit circle. The same self-configuring RISs as those used in Section 2.1 are added in the environment to spread the radiation pattern of the BS in the angular domain, and provide additional propagation paths in the environment, to reach the target UE. As illustrated in Figure 2-4, we compare the Equalized BF scheme to the MRT BF and the Reduced BF scheme (introduced in Section 2.1).

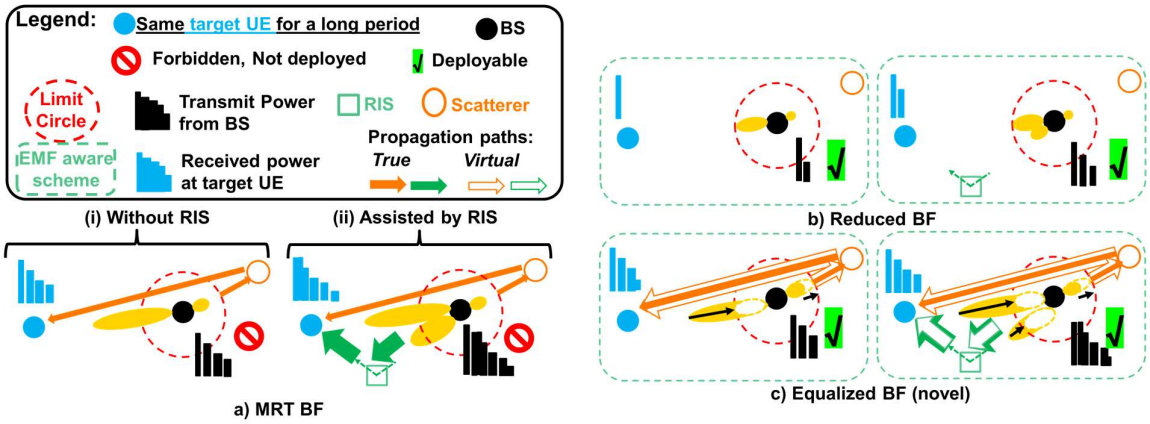

Figure 2-4 Studied BF schemes.

2.2.2 System Model

The same propagation model and RIS-aided BF procedures as in Section 2.1 are used. However, the RIS-aided BF procedure is slightly modified as follows, for the Equalized BF scheme. Instead of using the true CSI, the BS computes a virtual propagation channel as follows. As illustrated in Figure 2-5, the virtual propagation channel is computed based on a sounding of the true channel. Compared to the true channel, the virtual channel, has the same scatterers, in the same directions. However, the virtual channel, is equalized in the angular domain: the path gain of all scatterers is set to 1. As a consequence, the radiation pattern of the MRT BF will also be equalized in the angular domain. As in Section 2.1, the BS is assumed to perfectly know the channel between itself and locations on the limit circle. The BS therefore computes the transmit power to ensure that the EMFE constraint is met on the limit circle, with the Equalized BF precoder.
As in Section 2.1, the channel random parameters are drawn, and for each simulation sample, the following performance metrics are computed:

- The received power at the target UE.
- The BS transmit power.
- The percentage of positions exceeding the EMFE constraint beyond the limit circle (calculated inside a square surrounding the circle).

The mathematical details of the channel model and the procedures and simulation assumptions are provided in [APV+22-2].

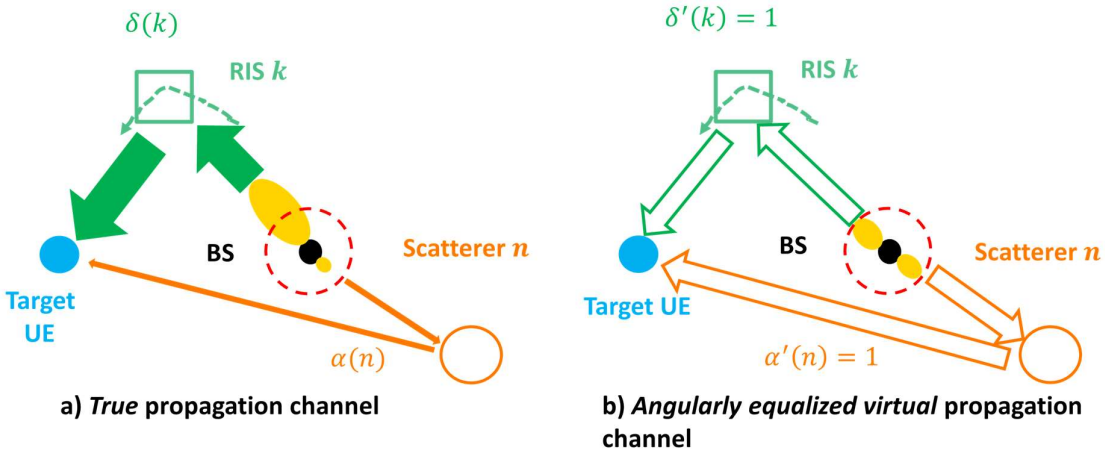

Figure 2-5 Angularly equalized virtual propagation model.

2.2.3 Results

Figure 2-6 illustrates statistics of the performance metrics introduced in 2.1.3, over random channels. Figure 2-6-a) illustrates the CDF of the percentage of positions exceeding the EMFE constraint (assuming the same UE is targeted for a long period), beyond the limit circle. Figure 2-6-b) illustrates the CDF of the BS transmit power and Figure 2-6-c illustrates the CDF of received power at the target UE. Performance with and without RIS assistance is plotted. MRT BF alone is not deployable. Reduced BF is compliant with the EMFE constrains but provides a low received power at the target UE. The Equalized BF scheme maximises the received power at the target UE and perfectly matches the constrain.

Detailed results and assumptions are available in [APV+22-2].

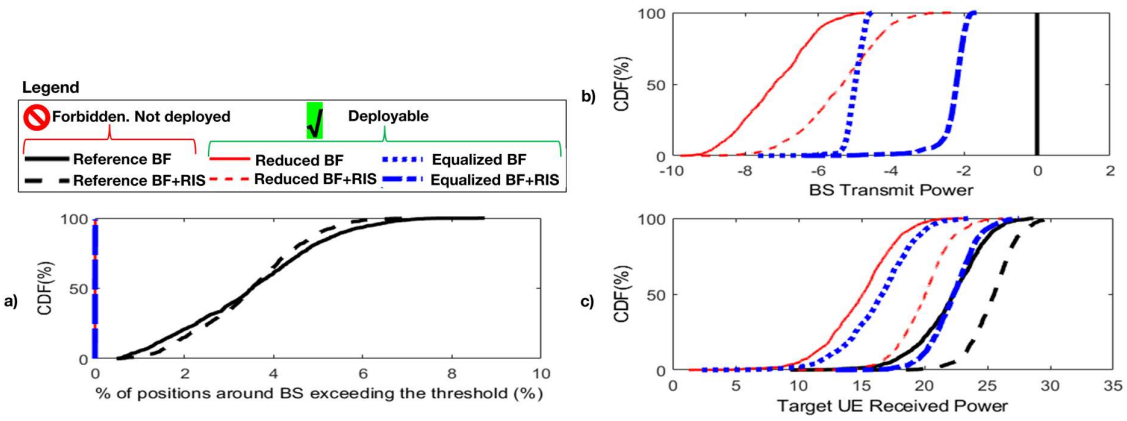

Figure 2-6 Results.

2.2.4 Conclusion

In this study, we propose a novel RIS-aided BF scheme called Equalized BF. It is built based on a virtual angularly equalized propagation channel. Equalized BF scheme provides a better throughput than Reduced BF scheme, and perfectly matches the EMFE constrain. Therefore, the proposed scheme boosts the inter-EMFEU.
Next studies will provide a comparison with the novel schemes presented in Section 2.1.

2.3 Inter-EMFE aware BF assisted by RIS: the MU-MIMO case

This section summarizes the work detailed in the submitted paper [YIP22].

2.3.1 Introduction

RISs are one of the key emerging 6G technologies that are expected to improve the link budgets between transmitters and receivers by adding artificial propagation paths. In such re-configured propagation environment, DL MU-MIMO brings capacity improvement to cellular networks. It benefits from the spatial dimension offered by MIMO systems to enable simultaneous transmission of independent data streams to multiple users on the same Radio Resources (RRs) by applying appropriate BF schemes. However, in some cases, serving the same subset of users for a long period of time may cause some undesired regions where the average EMFE exceeds the regulatory limits. To address this challenge, we propose a novel inter-EMF aware MU-MIMO BF scheme that aims to optimize the overall capacity under EMFE constraints in RIS-aided cellular networks. This work was submitted to the Globecom 2022 [YIP22].

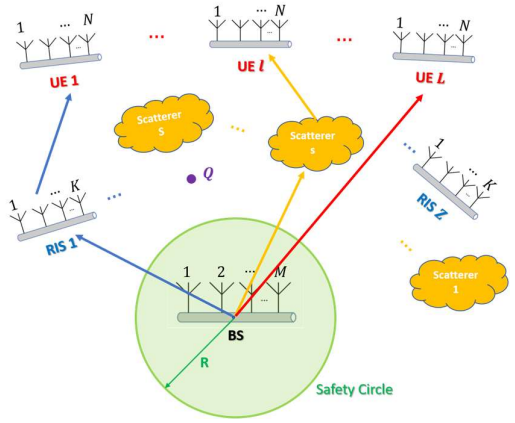

Figure 2-7 A MU-MIMO RIS-aided network model.

2.3.2 System Model

We consider the DL communication of a RIS-aided MU-MIMO network. As depicted in Figure 2-7, there are a BS and L different UEs in the cellular network, they are all equipped with multiple antennas. Assume that the BS has a linear antenna array of M antenna elements and each UE has N antenna elements. Thus, the total number of received antennas is $N_t = LN$. Those antenna elements are spaced by 0.5λ to the adjacent ones either on the BS or a single UE side, where λ indicates the wavelength of the carrier frequency. We assume that the BS must serve the UEs for a long period with the same BF scheme and power allocation, during the entire period. Therefore, the EMFE constrains must also be met instantaneously, to be met in average. Besides, there are S scatterers and Z RISs randomly located in the given space, respectively. Each RIS has a linear array of K elements with a spacing of 0.5λ. For simplicity, we consider here the far-field calculation method, i.e., both scatterers and RISs are far from the BS and the UEs. In the far-field, the electromagnetic waves propagate at the speed of light and electric and magnetic fields are mutually perpendicular.

Here, we consider an Orthogonal Frequency Division Multiplexing (OFDM) waveform and random Rayleigh fading. With spatial multiplexing, multiple streams are sent from the BS to distinct active UEs simultaneously, which are separated by using precoding schemes. In our case, the ZF linear precoding scheme adapted to multiple receiving antennas is applied. The network adopts TDD mode and thus the channel reciprocity is feasible.

First, the BF at the RIS side is selected based on the following procedure: (i) each UE sends some pilots which allow the RIS to estimate the UE-to-RIS channels, (ii) then based on this channel estimation, each RIS computes the BF reflection weight $w^z = \mathbb{C}^{K\times 1}$, reconfigures the weights and freezes. The phase shift weight is multiplied by a reflection amplitude r_{ris}, where $0 \leq r_{ris} \leq 1$ is a constant value depending on the hardware structure of the RIS. Here we set $r_{ris} = 1/K$. $r_{ris} = 1$ means that the RIS is reflecting as much as a natural scatterer. Once the RIS is configured, the UE sends pilots again, the BS can estimate the DL channel considering the RIS configuration and determine the appropriate BS BF to be used for data transmission.

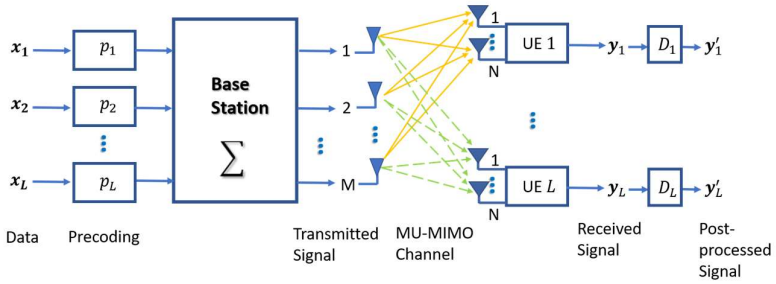

Figure 2-8 DL MU-MIMO Scheme.

2.3.3 Results

In this work, we focus on RIS-aided MU-MIMO scenario and aim to design efficient BF scheme to optimize the DL network capacity while satisfying EMFE constraints. In our scenarios, some RISs are randomly distributed as reflective surfaces to work on transmitting the incident signal to specified UE. First, we examine the "reference" MU-MIMO BF scheme that maximizes the DL capacity with full power transmission and without any EMFE constraint. It corresponds to a Zero-Forcing (ZF) precoding with a water-filling power allocation strategy. Then, we propose the "reduced" EMF-aware BF which consists of decreasing the overall transmit power until the EMFE limits are fulfilled. Moreover, we propose a novel "enhanced" EMF-aware BF with a per layer power control mechanism that is designed to meet EMFE constraints and achieve higher capacity performance. Here, we numerically evaluate the performance of the reduced and the enhanced EMF-aware BF schemes.

Name	Symbol	Value
Number of antenna elements at BS	M	64
Number of antennas at each UE	N	4
Number of RISs	Z	3
Number of Scatterers	S	3
Number of antennas at each RIS	K	4
Maximum transmit power	P_{max}	200 Watt
Radius of Safety Circle	R	50 m
EMFE threshold	EMF_{th}	-5 dBm

Table 2-1 Simulation Parameters.

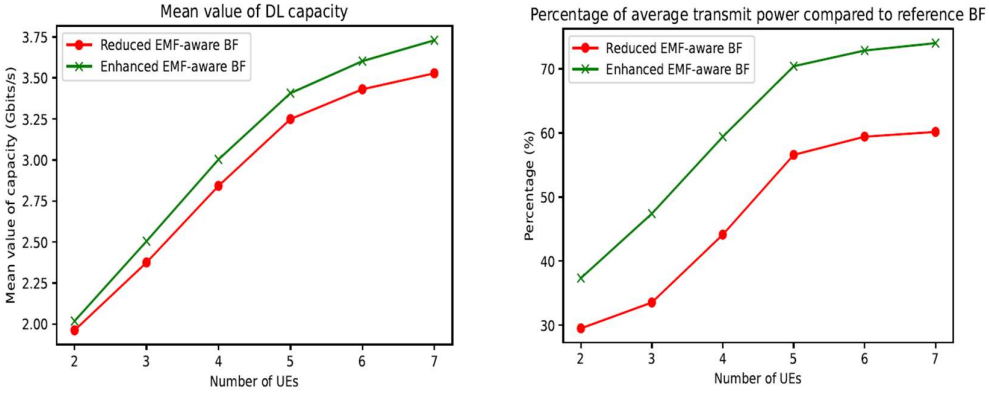

Figure 2-9 Numerical results.

We consider different number of UEs, i.e., from $L = 2$, to 7. There are 1000 samples of channels corresponding to each number L in the simulation. In Figure 2-9, the left figure plots the average DL capacity of the cellular network with respect to different BF schemes. The enhanced EMF-aware BF can maintain more than 70% of the capacity, which is 7% higher than the reduced BF. The right figure presents the percentage of average transmit power at the BS for the two proposed BF schemes compared to the reference BF. The enhanced EMF-aware BF can still guarantee the EMFE limits with about 10% higher transmit power than the reduced one.

2.3.4 Conclusion

In this work, we modelled the DL communication in a RIS-aided MU-MIMO systems. Two BF schemes are proposed to address EMFE regulation: (i) reduced and (ii) enhanced EMF-aware MU-MIMO BF. We compare the simulation performance of these two schemes. The enhanced EMF-aware scheme achieves a higher system capacity compared to the reduced one which has a lower average transmit power. In the near future, we will jointly optimize the transmit precoding weight and the power allocation scheme in order to achieve higher capacity performance while satisfying EMFE regulation. Therefore, the proposed scheme boosts the inter-EMFEU.

2.4 The RIS opportunity to reduce EMFE, using optimization tools

This section summarizes the work detailed in the submitted paper [ACS22].

2.4.1 Introduction

In this study, we investigate the synergy between RISs and multi-access edge computing (MEC)-aided wireless networks for enabling computation offloading tasks via low EMF communications.
We consider for this purpose an RIS-assisted scenario of MIMO system aware BF. We focus on the typical case of computation offloading, i.e., the UL traffic, which generally pertains to the continuous transfer of capillary data from extreme edge devices such as sensors and cars, to enable computational demanding services in real-time, at the edge of wireless communication networks. This drastic growth calls indeed, for new optimization metrics that include energy, service delay, and EMFE.
In line with this, we deal in this analysis with the EMFE under end-to-end delay constraints of a computation offloading service. We formulate thus, the blue (i.e. low EMFE) communications edge computing problem as a long-term optimization aiming to minimize the average EMFE, as per ICNIRP recommendations, under MEC service delay constraints. We design an online algorithm able to dynamically configure RIS parameters, transmitter precoding, receiver combiner, and transmit power, with theoretical guarantees on system stability and asymptotic EMFE optimality. Note that, precoding, combining, and RIS parameters are selected from generic codebooks.

2.4.2 Description and objective

System Model

We consider a MIMO system where a single user aims to offload his computation tasks to a mobile edge host (MEH) collocated at his serving access point (AP), through an RIS-aided wireless link. We consider time as organized in slots $\tau = 1, 2, \ldots$ of equal duration τ. At the beginning of each slot, new offloading data are generated, new radio channels are observed and, based on these and other observations, a new resource allocation decision is taken. Accordingly, while instantaneous instances of the EMFE may reach high values, the long-term average is finally minimized to achieve low exposure, under service delay guarantees.

General optimization problem

As illustrated in Figure 2-10, for EMFE evaluation, space is considered as divided in pixels of equal size. Then, assuming that humans possibly exist in one or more of these pixels, our objective is to minimize a weighted sum of the EMFE in each pixel. In this way, if humans are not generally present in one pixel, the EMFE problem can be neglected in that particular location in space, assigning weight 0. This way, it is possible to customise on a case-by-case need.

- **The p-th pixel EMFE:**

In this case, we deal with the scenario of one human placed in pixel p, then, the objective becomes the p-th pixel EMFE, to achieve a blue communication area. Note that, this is the example represented in the numerical results. Otherwise, the overall method is more general and applies to multiple humans sojourning in multiple pixels. To cope with ICNIRP recommendations [ICN20], we consider the incident power density, as a metric for EMFE evaluation. Then, taking into account, the impact of both the direct and the reflected paths, we represent the overall instantaneous power density as

$$P_{d,p}(t) = \frac{4\pi}{\lambda^2} P_{tx}(t) \left| h_p(t) w_u(t) \right|^2$$

Where $h_p(t) = h_{d,p}(t) + h_{r,p}(t)\Theta(t)H_{u,r}(t)$ is representing the overall channel between the user and pixel p, comprising both the direct channel vector between the UE and pixel p and the channel vector between the RIS and pixel p. w_u is the user precoding vector and P_{tx} is the

user transmit power at time t. As already mentioned, the goal of this investigation is to minimize the long-term average EMFE in selected areas across space under service delay constraints, by dynamically and adaptively controlling the user precoding vector, the transmit power, the RIS reflectivity parameters, and the combining vector.
Then thanks to the theoretical foundations of Lyapunov stochastic optimization, we decompose a long-term complex optimization problem and solve it in a per-slot basis, thus performing an exhaustive search over the codebooks (designed for the precoder, the combiner, and the RIS parameters), with corresponding closed form solutions for the transmit power. This is possible thanks to the definition of a suitable function (an instantaneous objective that weights service queue states and EMFE) to be minimized in each time slot, based only on instantaneous observations. This guarantees the queue stability constraints (communication and computation buffers), while asymptotically approaching the global optimal solution through one tuning parameter that trades off average EMFE optimality and service delay.

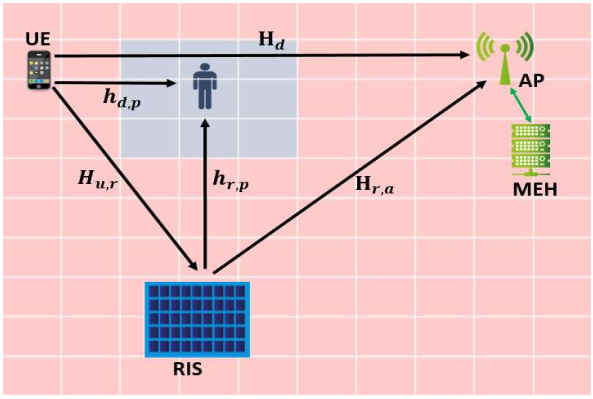

Figure 2-10 System Model.

2.4.3 Results

The antenna patterns used to build w_u, w_a, and T (respectively, the precoder, the combiner, and the RIS codebooks), are taken from [RH10], with each element modelled as in [CLS+12]. A range of -60° to 60°, with a step of 10° is considered for the UE and the AP, while a range of -30° to 30° with a step of 5° is considered for the RIS, with 0° the direction perpendicular to the array. At the MEC side, we assume the MEH to be able to accommodate all requests on average, however with an instantaneous random f(t) (the amount of resources in central processing unit (CPU) cycles/s) uniformly distributed. In particular, denoting by (x, y, z) the three-dimension (3D) coordinates of an element, we model the scenario deployment depicted in Figure 2-10 using the following positions: the AP at (50,50,1), the UE at (0,50,1), the RIS at (4,48,1), and the man at (1,50,1).

Name	Symbol	Value
Bandwidth	B	800 MHz
Carrier frequency	f	28 Ghz
Noise power spectral density	N0	-174 dBm/Hz
Slot duration	τ	10 ms
Arrival rate	$A_k(t)/s$	10 Gbps
The user maximum transmit power	P_{tx}^{max}	100 mw
Transmit and receive antennas	N_u and N_a	8
RIS elements	M	20

Table 2-2 Simulation Parameters

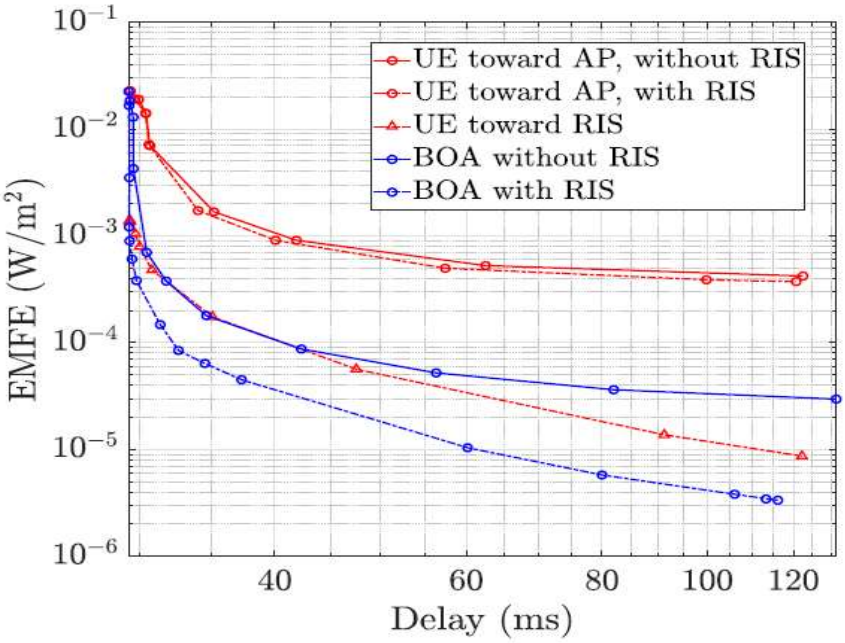

Figure 2-11 Results.

Numerical results show the effectiveness of our method and the benefits of the RIS in enabling blue communications for computation offloading services, due to which the UL direction of communication will be exploding in future 6G systems.
For instance, as one of obtained results, Figure 2-11, shows the trade-off between the EMFE and the average end-to-end (E2E) delay. For this simulation, we consider four different benchmark comparisons: i) the no RIS aided case, with the UE always transmitting towards the AP, and with transmit power optimized; ii) the RIS-aided case, with the UE always transmitting towards the AP, and with transmit power optimized; iii) the RIS-aided case, with the UE always transmitting towards the RIS, and with transmit power optimized; iv) the case without the RIS, but applying our optimization method. Finally, we term our full optimization algorithm as BOA (blue optimization algorithm). Results show how the use of the RIS offers the opportunity to reduce the level of EMFE for a given service delay, also in the case the UE always transmits towards the RIS. However, this gain is considerably enhanced when BOA is applied, due to the increased degrees of freedom introduced by the adaptive selection of precoding, combining, and RIS parameters.

2.4.4 Conclusion

We proposed an online method able to adaptively and jointly optimize precoding, combining, RIS parameters, and transmit power in a RIS-aided MEC offloading scenario. As objective, we considered the average EMFE in selected areas within the service coverage, with constraints on the E2E service delay. We reduced a long-term problem to a per slot optimization, which allowed us to solve it through a low complexity procedure involving an exhaustive search over low cardinality sets, coupled with a closed form solution for the transmit power.
Therefore, the proposed scheme boosts the inter-EMFEU.

2.5 EE Optimization of Reconfigurable Intelligent Surfaces with self-EMFE Constraints

This section summarizes a study that is detailed in [ZR22].

2.5.1 Introduction

This work considers the problem of EE maximization in a RIS-based communication link, subject to not only the conventional maximum power constraints, but also additional constraints on the maximum exposure to electromagnetic radiations of the end users. In [IEA+22], EMF-aware scheme for RIS-based wireless networks has recently been developed. Therein, the users' electromagnetic exposure is minimized subject to quality-of-service constraints. Instead, in this work we consider a different, more general problem of maximizing the EE in an RIS-assisted communication MIMO link, enforcing both maximum power constraints and maximum EMFE constraints. The optimization problem is tackled with respect to the RIS phase shifts, the transmit BF, the linear receive filter, and the transmit power. The EMF constraints are formulated in terms of maximum acceptable values for the specific absorption rate (SAR), which measures the rate of electromagnetic energy absorption per unit mass of human body when it is exposed to a radio frequency electromagnetic field [W+11][C+21].

2.5.2 System Model

Consider a single-user system in which a transmitter with N_T antennas and a receiver with N_R antennas communicate through an RIS. The direct link between the transmitter and receiver is assumed to be weak enough to be ignored. Denote by the end-to-end path loss, H and G the fading channels from the transmitter to the RIS and from the RIS to the receiver, respectively, p the transmit power, q and w the unit-norm transmit beamformer and receive combiner. The RIS has N elementary passive scatterers, which can independently reflect the radio wave impinging upon them according to a unit amplitude reflection coefficient $e^{j\phi_n}, n = 1, \dots, N$ and j denoting the imaginary unit. Under these assumptions, the system bit-per-Joule EE is expressed as

$$EE = \frac{B\ log_2(1+\frac{p}{\delta\sigma^2}|w^H G \boldsymbol{\Phi} H q|^2)}{\mu p + P_c} \quad \textbf{(2.5.1)}$$

with μ the inverse of the transmit amplifier efficiency, P_c the static power consumption of the system, B the communication bandwidth, and σ^2 the receive noise power.

The objective of this work is to optimize the RIS matrix $\boldsymbol{\Phi}$, the BF vector q, the receive filter w, and the transmit power p, for EE maximization, subject to both power and EMF constraints.

$$\max_{\boldsymbol{\Phi},q,w} \ EE \quad \textbf{(2.5.2)}$$

$$S.t. \quad \phi_n \in [0,2\pi], \qquad 0 \le p \le P_{max}$$

$$\sum_{n=1}^{N_T} c_n|q_n| \le P_q\,, \sum_{n=1}^{N_T} |q_n|^2 \le 1$$

$$\sum_{n=1}^{N_R} d_n|w_n| \le P_w\,, \sum_{n=1}^{N_R} |w_n|^2 \le 1$$

wherein P_{max} is the maximum transmit power, P_q and P_w are the maximum EMF constraints at the transmitter and receiver side, respectively, while $\{c_n\}_{n=1}^N$ and $\{d_n\}_{n=1}^N$ are the EMF absorption coefficients.

A suitable approach to tackle Problem (2.5.2) is the alternating optimization (AO) of the RIS phase shift matrix $\boldsymbol{\Phi}$, the BF vector q, the receive filter w, and the transmit power p. The overall optimization algorithm can be stated as in Algorithm 1.

Algorithm 1 Alternating maximization

Initialize $\boldsymbol{w}$ and $\boldsymbol{q}$ to feasible values.
repeat
  $\boldsymbol{g} = \boldsymbol{w}^H \boldsymbol{G}$; $\boldsymbol{h} = \boldsymbol{H}\boldsymbol{q}$; $\phi_n = -\angle g_n^* h_n$, $\forall n = 1, \ldots, N$;
  $\boldsymbol{v}^H = \boldsymbol{w}^H \boldsymbol{G}\boldsymbol{\Phi}\boldsymbol{H}$; $q_n = x_n e^{j\angle v_n}$, $\forall n = 1, \ldots, N$, with $\boldsymbol{x}$ the solution of Problem (3);
  $\boldsymbol{u} = \boldsymbol{G}\boldsymbol{\Phi}\boldsymbol{H}\boldsymbol{q}$; $w_n = y_n e^{j\angle u_n}$, $\forall n = 1, \ldots, N$, with $\boldsymbol{y}$ the solution of Problem (4);
until Convergence
Set p as the solution of (5);

$$\max_{\{x_n \geq 0\}_n} \sum_{n=1}^{N_T} |v_n| x_n \quad , s.t. \sum_{n=1}^{N_T} c_n x_n \leq P_q \, , \sum_{n=1}^{N_T} {x_n}^2 \leq 1 \qquad (3)$$

$$\max_{\{y_n \geq 0\}_n} \sum_{n=1}^{N_R} |u_n| y_n \quad , s.t. \sum_{n=1}^{N_R} d_n y_n \leq P_w \, , \sum_{n=1}^{N_R} {y_n}^2 \leq 1 \qquad (4)$$

$$\max_{p} \frac{log_2(1+pc)}{\mu p + P_c} \quad s.t. \;\; 0 \leq p \leq P_{max} \qquad (5)$$

$$where \; x_n = |q_n| \, , v^H = \; w^H G \boldsymbol{\Phi} H, y_n = |w_n| \, , u = \; G \boldsymbol{\Phi} H q \;\; and \; c = \frac{|w^H G \boldsymbol{\Phi} H q|^2}{\delta \sigma^2}$$

A special case of problem (2.5.2) is for typical co-located multi-antenna devices where the human body has the same SAR for every antenna of the array. The global optimization of this special case can be stated as in Algorithm 2.

Algorithm 2 Global optimization with $P_q/c \leqslant 1$, $P_w/d \leqslant 1$.

for $i = 1$ **to** N_T **do**
  for $j = 1$ **to** N_R **do**
    $n_q = i$; $n_w = j$; Obj$(i,j) = \sum_{n=1}^{N} |\boldsymbol{g}_{n_w}(n) \boldsymbol{h}_{n_q}(n)|$;
  end for
end for
$(n_q^o, n_w^o) =$ argmax Obj(i,j);
$\boldsymbol{q} = \frac{P_q}{c}[\underbrace{0, \ldots, 0}_{n_q^o - 1}, 1, 0, \ldots, 0]$; $\boldsymbol{w} = \frac{P_w}{d}[\underbrace{0, \ldots, 0}_{n_w^o - 1}, 1, 0, \ldots, 0]$;
$\phi_n = -\angle g_{n_w^o}(n) h_{n_q^o}(n)$; Set p as the solution of (5);

2.5.3 Results

In our numerical analysis, we set $B = 5\,MHz$, $\delta = 110\,dB$, $N_0 = -174\,dBm/Hz$, $N_T = N_R = 4$, $P_c = 30\,W$, $P_{max} = 20\,W$. As for the fading channels, a Rician model is considered, wherein $h_n \sim \mathcal{CN}(v_h, 1)$ and $g_n \sim \mathcal{CN}(v_g, 1)$ with v_h and v_g such that the power of the line-of-sight path is four times larger than the power of all the other paths. All results are averaged over 10^3 independent channel realizations. Moreover, $c_n = c = {}^1/_{N_T}$ and $d_n = d = {}^1/_{N_R}$. For simplicity, thus, we consider the isotropic EMF setup. Figure 2-12 and Figure 2-13 show the system EE and the EMFE $c\sum_{n=1}^{N} |q_n|$, respectively, as a function of ${}^{P_q}/_c$ for $N = 100$, and as a function of

N for $P_q/c = 0.85$. From Figure 2-12 and Figure 2-13, we observe that enforcing an EMF constraint on the SAR of the human body reduces the EE level, since it restricts the feasible set of the problem. The use of RISs offers, however, the opportunity of achieving the desired EE while ensuring SAR compliant communications. Figure 2-12 shows that, by increasing N, we can attain the same EE as the benchmark systems in the absence of EMF constraints.

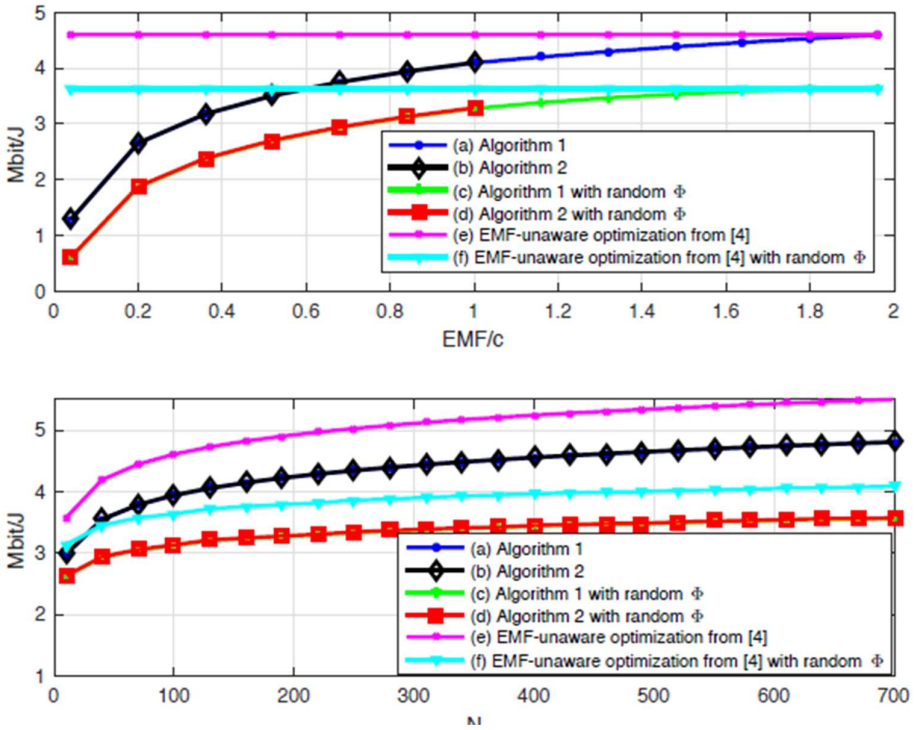

Figure 2-12 Average EE as a function of (top) P_q/c for $N = 100$ and (bottom) N for $P_q/c = 0.85$.

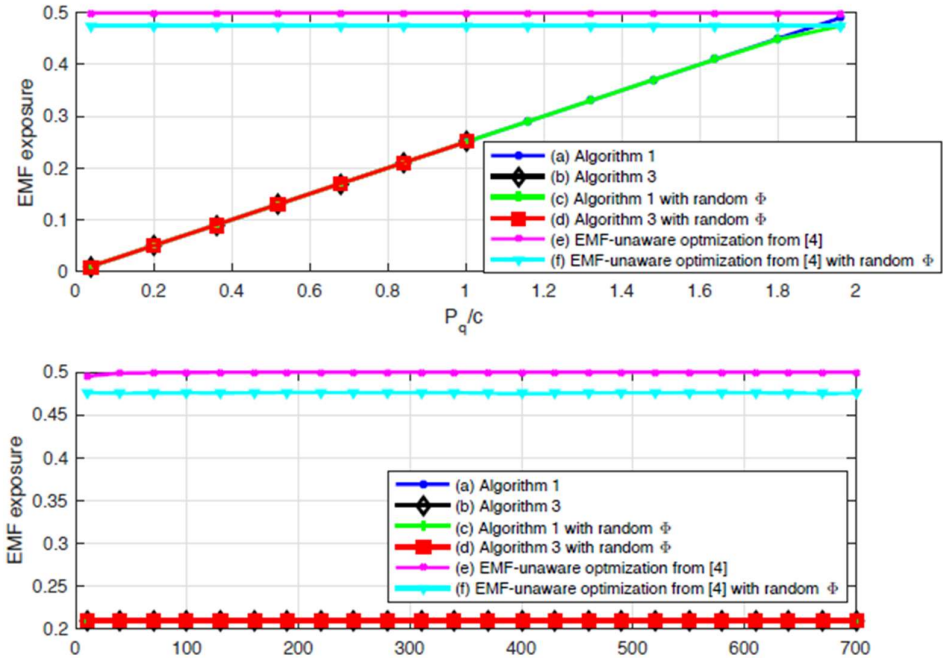

Figure 2-13 EMF constraint as a function of (top) P_q/c for $N = 100$ and (bottom) N for $P_q/c = 0.85$.

2.5.4 Conclusion

Low-complexity optimization algorithms have been proposed for EE maximization subject to EMF constraints. The analysis has shown that the use of a RIS can keep under control the end-users' EMFE while ensuring the desired EE level. Notably, this is obtained by using nearly passive RISs that do not increase the amount of electromagnetic radiation over the air. Thus, the proposed scheme boosts the self-EMFEU and the EE.

2.6 RIS Solution for enhanced EE and EMFEU

This section summarizes a study that will be detailed in the paper under preparation [GS+22].

2.6.1 Introduction

5G and beyond systems call for improved service qualities in terms of, e.g., data rate, EE, and latency. With more radio resources at millimeter wave (mmWave) or even THz frequencies, more opportunities have been revealed to improve the end-to-end throughput and at the same time, reach good trade-off with EE. However, signals at high frequencies can be significantly affected by the penetration loss, together with severe path loss and BF mismatch. State-of-the-art research studies on, e.g., advanced massive MIMO BF, deploying small cells, and various spatial and temporal resource allocation methods, could reach different performance-complexity trade-offs. From another perspective, these advanced wireless communication schemes trigger renewed attention to EMFE from both regulation authorities and populations. Although currently there is no scientific evidence that EMFE could have adverse effects on the environment and the population health at levels below what is already regulated, it is becoming more and more important to design sustainable and health-guaranteed wireless systems to satisfy both current and potential strict regulations due to increasing public acceptance requirements.

RIS has emerged as a promising future technical candidate thanks to its capabilities to program the radio environment and utilizing the desired propagation paths. It is extremely helpful when the direct link from the access point to a user faces deep fading and/or blockage. Moreover, with a proper deployment, RIS can cover different areas with different service requirements, which makes it possible to bypass certain blockage/users with no need for handover, backhauling, and wired energy supply. Inspired by these features, with the EMF aspect being considered, one can use RIS to create additional paths to avoid exceeding EMF powers in certain area or directions.

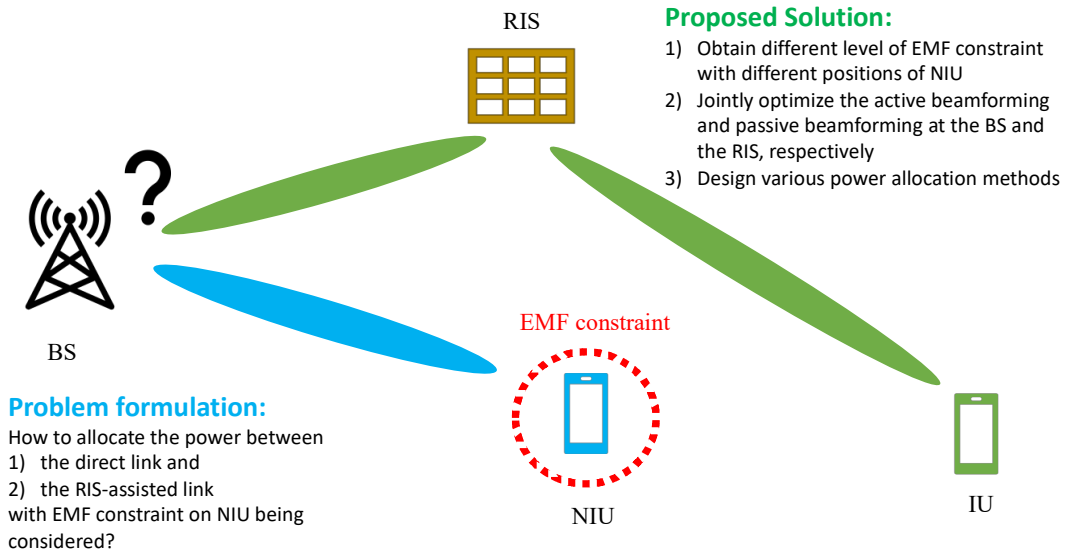

Figure 2-14 Problem and proposed solution.

Recent research studies have addressed the BF design at both the BS and the RIS with limited beam power requirements as EMF constraints. In this work, we consider various cases, where the relative positions of the non-intended user (noted NIU in this current sub-section) with respect to the intended user (noted IU in this current sub-section) are different. Specifically, we investigate the potential of EMF-constrained RIS-assisted networks with proper power allocation between the direct BS-IU and the in-direct BS-RIS-IU paths. The problem formulation and the contributions can be seen in Figure 2-14.

2.6.2 System Model

We consider a small cell outdoor BS/AP operating with mmWave carrier frequencies. As illustrated in Figure 2-15, we consider an RIS-assisted DL MIMO network with one BS (N_T antennas), one RIS (N elements) and a pair of single-antenna IU and NIU. Here, IU is the user who wants to receive service from the BS while the NIU has no need to connect to the BS. More importantly, NIU prefers to have limited EMFE given that it has no communication service. The NIU moves between the BS and the IU. Depending on the location of the NIU and the beam width from the BS, at some points/areas the NIU and IU receive the same transmission from the BS. We assume that the NIU does not decode the message or absorb the energy from the BS. RIS is assumed to be in the far field of target UEs and the BS. TDD mode is assumed, where perfect CSI could be obtained from channel reciprocity.

As illustrated in Figure 2-15, we jointly optimize the RIS and the BS BF for the intended user, given that a non-intended user moves between the BS to the intended user along the x-axis, with some EMF constraints. Targeting on maximizing the data rate at the IU with limited power budget, we propose a closed-loop scheme based on the feedback from NIU with the direct link being considered, in order to fully explore the potential of RIS-assisted systems with EMF constraints. Hence, this scheme aims at improving the EMFEU metric.

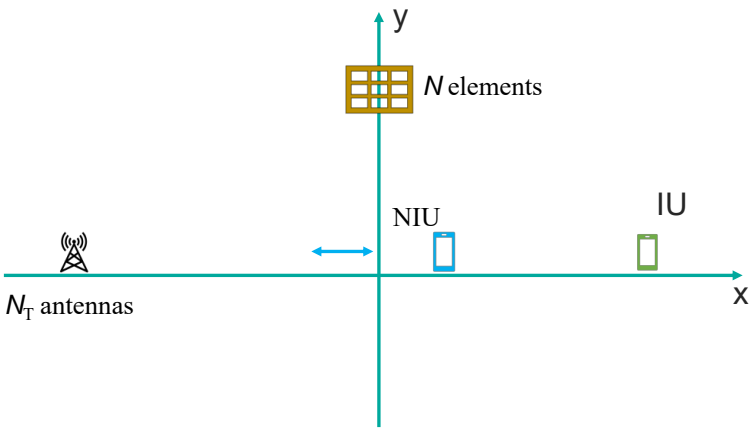

Figure 2-15 System Model

In some scenarios, especially with large number of elements in RISs, computing the phase coefficients at the RIS and precoder at the BS with explicit CSI may not be practical. Inspired by the precoding scheme with predefined codebooks, we propose to use a DFT codebook-based beam optimization where the RIS beam is selected from the pre-defined beam patterns while only the BS-RIS-IU concatenated channel is required to obtain the optimal beam. We

compare the proposed DFT-based beam optimization with the state-of-the-art AO scheme where the full knowledge of CSI is required.

2.6.3 Expected Results

Here, we present the numerical results of considered power allocation schemes:

- Method 1: Allocate all power to the BS-RIS-IU link (DFT optimization)
- Method 2: Allocate all power to the direct link, with respect to the EMF constraint
- Method 3: First fill the direct link with the maximum possible power with respect to the EMF constraint, then transmit the remaining power to the BS-RIS-IU
- Method 4: Exhaustively find the best power allocation considering the EMF constraint
- Upper bound: No EMF constraint and transmit with the direct link

Name	Symbol	Value
Transmit antenna at BS	N_T	32
RIS elements	N	100
Carrier frequency	f_c	28 GHz
Bandwidth	B	100 MHz
Noise power	N_0	-174 dBm/Hz with 10 dB noise figure
EMF constraint	$\bar{P}$	0.1 mW
Total power	P	43 dBm
BS position	-	[-80m, 0]
RIS position	-	[0, 50m]
IU position	-	[80m, 0]

Table 2-3 Simulation Parameters.

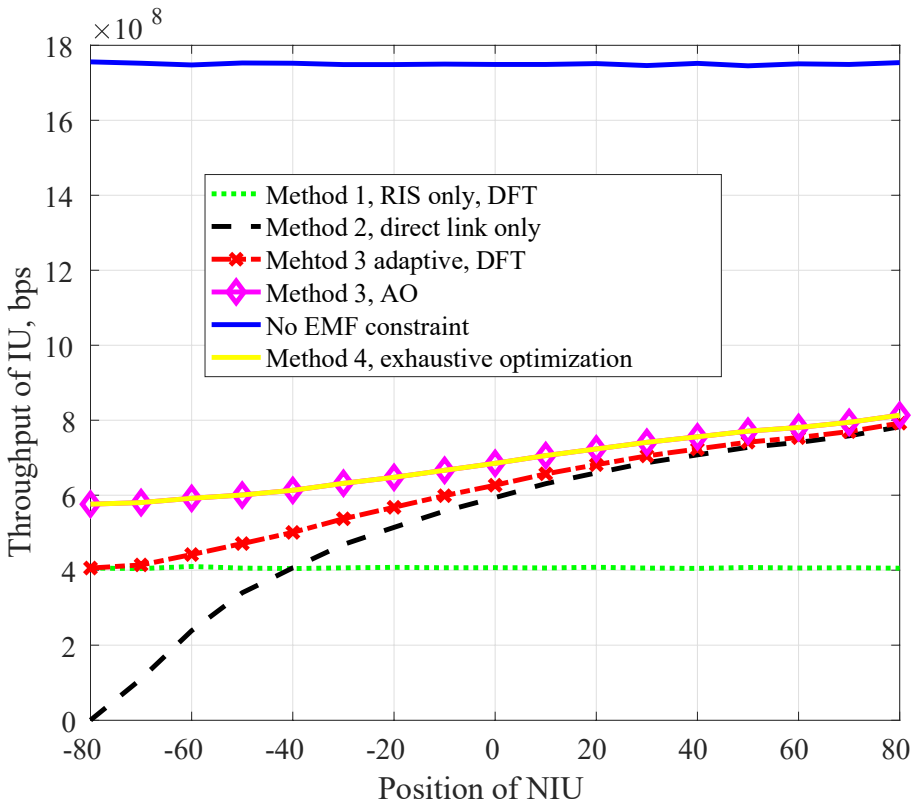

Figure 2-16 Expected results.

2.6.4 Conclusion

We designed an RIS-assisted EMF-constrained system with the same beam for both IU and NIU, and we designed different power allocation methods for the direct and RIS-assisted links. To optimize the RIS, we designed both AO- and DFT-based methods that can reach similar performance with full/limited CSI. Our results indicate that, although the EMF constraint would strongly benefit from an additional RIS link to meet the performance requirements of the IU, depending on the position of the NIU, the direct link is still useful to further improve the performance. Therefore, the proposed scheme boosts the inter-EMFEU.

2.7 Energy efficiency maximization of MMIMO communications with dynamic metasurface antennas

This section summarizes the work detailed in papers [YXA+21-1], [YXA+21-2].

2.7.1 Introduction

In this study, we investigate the optimization of the EE performance of Dynamic Metasurface Antennas (DMA)-assisted [SAI+21] massive MIMO wireless communications on the uplink direction. We consider the joint design of the transmit precoding of each multi-antenna user and the DMA tuning strategy at the BS to maximise the EE performance, considering the availability of either instantaneous or statistical CSI. Specifically, the proposed framework is shaped around Dinkelbach's transform, AO, and deterministic equivalent methods. In addition, we obtain a closed-form solution to the optimal transmit signal directions for the statistical CSI case, which simplifies the corresponding transmission design for the multiple-antenna case.

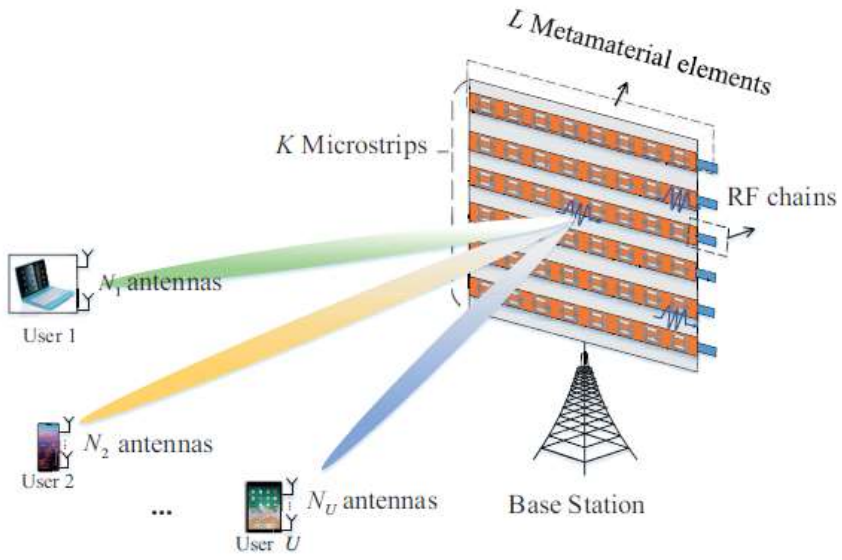

Figure 2-17 The considered DMA-assisted massive MIMO uplink system.

2.7.2 System Model

We consider a single-cell massive MIMO uplink system where the BS simultaneously receives signals from multiple users. In the following, we illustrate the input-output relationship of DMAs and the channel model.

The considered system is composed of a DMA-based BS and U users. The BS is equipped with a planar array consisting of M metamaterial elements, and each user is equipped with N_u conventional antennas in a fully digital architecture. We assume that the DMA array consists of K microstrips, e.g., the guiding structure whose top layer is embedded with metamaterials, and each microstrip consists of L metamaterial elements, that is, $M = KL$. Each metamaterial element observes the radiations from the channels, adjusts, and transmits them along the microstrip to the corresponding RF chain independently. The output signal of each microstrip is

the linear combination of all the radiations observed by the corresponding L metamaterial elements. The output signals of DMAs can be formulated as

$$\boldsymbol{z} = \boldsymbol{QHy} \tag{2.7.1}$$

where $\boldsymbol{y}$ denotes the DMA input signals, $\boldsymbol{H}$ is a diagonal matrix with entries the filter coefficients of the lth metamaterial in the kth microstrip, and $\boldsymbol{Q}$ is the configurable weight matrix of DMAS. In particular,

$$(\boldsymbol{Q})_{\{k_1,(k_2-1)L+l\}} = \begin{cases} q_{\{k_1,l\}}, k_1 = k_2 \\ 0, \ k_1 \neq k_2 \end{cases}, \tag{2.7.2}$$

where $q_{\{k_1,l\}}$ is the gain of the lth metamaterial in the k_1th microstrip. We also define $\boldsymbol{x}_u$ as the transmit signals from user u with zero mean and the transmit covariance matrix $E\{\boldsymbol{x}_u\boldsymbol{x}_u^H\} = \boldsymbol{P}_u$. Additionally, $\boldsymbol{x}_u$ satisfies $E\{\boldsymbol{x}_u\boldsymbol{x}_{u'}^H\} = \boldsymbol{0}, \forall\, u \neq u'$, which indicates that the signals from different users are independent of each other. Then, the channel output signal $\boldsymbol{y}$ is given by

$$\boldsymbol{y} = \sum_{u=1}^{U} \boldsymbol{G}_u\boldsymbol{x}_u + \boldsymbol{n}\,, \tag{2.7.3}$$

where $\boldsymbol{G}_u$ denotes the channel between user u and the BS, and $\boldsymbol{n}$ denotes the independently and identically distributed (i.i.d.) noise with covariance $\sigma^2\boldsymbol{I}_M$, where σ^2 denotes the noise power.

2.7.3 Problem Formulation with Instantaneous CSI

The objective of this section is to design the transmit covariance matrices $\boldsymbol{P}_u$, and the DMA weight matrix $\boldsymbol{Q}$ to maximize the system EE performance, considering instantaneous CSI [VAT18], [VAT19]. To define the system EE, we start with the Spectral Efficiency (SE) definition of the DMA-assisted uplink system. Assume that all metamaterial elements have the same frequency selectivity, then $\boldsymbol{H}$ can be expressed as the identity matrix multiplied by a constant. Therefore, the achievable system SE is given by

$$R = \log_2\left|I_K + \frac{1}{\sigma^2}\sum_{u=1}^{U} \boldsymbol{Q}\,\boldsymbol{G}_u\boldsymbol{P}_u\boldsymbol{G}_u^H\boldsymbol{Q}^H(\boldsymbol{QQ}^H)^{-1}\right|. \tag{2.7.4}$$

The whole power consumption of the DMA-assisted system is given by

$$W = \sum_{u=1}^{U}(\xi_u tr(P_u) + W_{c,u}) + W_{BS} + KW_S, \tag{2.7.5}$$

where $\xi_u = \rho_u^{-1}$ with ρ_u denoting the transmit power amplifier efficiency of user u. In addition, $W_{c,u}$ denotes the static circuit power dissipation of user u and W_S represents the dynamic power dissipation of each RF chain chain, including, e.g., power consumption in the ADCs, amplifier, and mixer. W_{BS} incorporates the static circuit power dissipation at the BS. With the system SE in (2.7.4) and power consumption in (2.7.5), the EE of our considered DMA-assisted uplink system is defined as

$$EE = B\frac{R}{W}, \tag{2.7.6}$$

where B is the channel bandwidth. So far, the EE maximisation problem of the DMA-assisted uplink system by designing the transmit covariance matrices $\boldsymbol{P}_u, \forall\, u$, and DMA weight matrix $\boldsymbol{Q}$ is formulated as follows:

$$\max_{\mathbf{Q},\mathbf{P}} \ EE \tag{2.7.7}$$

$$s.t. \quad (2.7.2),$$

$$tr(\boldsymbol{P}_u) \leq P_{max}\,, \boldsymbol{P}_u \succcurlyeq \boldsymbol{0},$$

where P_{max} denotes the maximum available transmit power.

To solve the optimization problem (2.7.7), we adopt an AO method to design $\boldsymbol{P}$ and $\boldsymbol{Q}$ in an alternating manner. For the optimization of $\boldsymbol{P}$, we adopt Dinkelbach's transform to convert the concave-linear fraction in the constraint (2.7.2) into a concave one. For the optimization of $\boldsymbol{Q}$, we first neglect the second set of constraints (related to $\boldsymbol{P}$) to obtain the corresponding unconstrained **Q**, and then adopt an alternating minimisation algorithm to reconfigure **Q** to be constrained by (2.7.2).

2.7.4 Problem Formulation with Statistical CSI

Channels might be fast time-varying in practical wireless communications, thus frequently tuning DMAs and reallocating transmit power with instantaneous CSI might be difficult. In such cases, utilizing statistical CSI to optimize the system EE performance is more efficient. In this section, we explore approaches to optimize the system EE by designing the transmit covariance matrices and DMA weight matrix via exploiting statistical CSI.

To formulate the corresponding EE maximization problem, we firstly describe the system SE and power consumption metrics. For the statistical CSI case, we adopt the ergodic achievable SE metric defined as:

$$\bar{R} = E\left\{\log_2\left|I_K + \frac{1}{\sigma^2}\sum_{u=1}^{U}\boldsymbol{Q}\,\boldsymbol{G}_u\boldsymbol{P}_u\boldsymbol{G}_u^H\boldsymbol{Q}^H(\boldsymbol{Q}\boldsymbol{Q}^H)^{-1}\right|\right\}, \quad \textbf{(2.7.8)}$$

where the expectation is taken over the channel realisations. In addition, we use (2.7.5) to model the overall power consumption. Then, the corresponding EE maximization problem can be formulated in a similar manner with the instantaneous CSI problem (2.7.7), using (2.7.8). However, it is challenging to tackle because the objective exhibits a concave-linear fractional structure. In addition, the expectation operation further increases the computational overhead. Nevertheless, this optimization problem can be solved by first deriving an optimal closed-form solution to the transmit signal directions of users. Then, we apply the deterministic equivalent method to asymptotically approximate the ergodic SE, aiming to reduce the computational overhead. Next, we adopt Dinkelbach's transform to obtain the users' power allocation matrices. Finally, we derive the weight matrix of DMAs with a similar method to the instantaneous CSI case.

2.7.5 Results

In our numerical analysis, we set the number of users as $U = 6$ and each user is equipped with 4 antennas, i.e., $N_u = 4, \forall u \in U$. The antennas of users are placed in uniform linear arrays spaced with half wavelength. We set the number of microstrips as $K = 8$ and each microstrip is embedded with $L = 8$ metamaterial elements. The space between metamaterial elements on the DMA array is set as 0.2 wavelength. We set the bandwidth as $B = 10\,MHz$, the amplifier inefficiency factor as $\rho = 0.3, \forall u$, and the noise variance as $\sigma^2 = -96\,dBm$. For the power consumption, we set the static circuit power as $W_{c,u} = 20\,dBm, \forall u$, the hardware dissipated power at the BS as $W_{BS} = 40\,dBm$, and the static power per microstrip as $W_S = 30\,dBm$. Additionally, the entries of the DMA weight matrix Q are selected from the following four sets [SDE+19]:

- UC: the complex plane, i.e., $Q = C$;
- AO: amplitude only, i.e., $Q = [0.001, 5]$;
- BA: binary amplitude, i.e., $Q = \{0, 0.1\}$;
- LP: Lorentzian-constrained phase, i.e., $Q = \left\{\frac{1+e^{J\phi}}{2} : \phi \in [0, 2\pi]\right\}$.

In Figure 2-18, the DMA weights are chosen from the complex-plane set. We compare the EE performance of the DMA-assisted uplink system versus the power budget Pmax between the instantaneous and statistical CSI cases. As expected, the EE performance is better when the instantaneous CSI can be perfectly known in both the EE- and SE-oriented approaches. We also observe that the EE performance based on statistical CSI is quite close to that based on instantaneous CSI. Note that, the optimization process in the statistical CSI case is more computationally efficient than the instantaneous CSI one. Thus, in our DMA-assisted communication scenario, the statistical CSI is a good substitute for the instantaneous CSI to maximize the system EE.

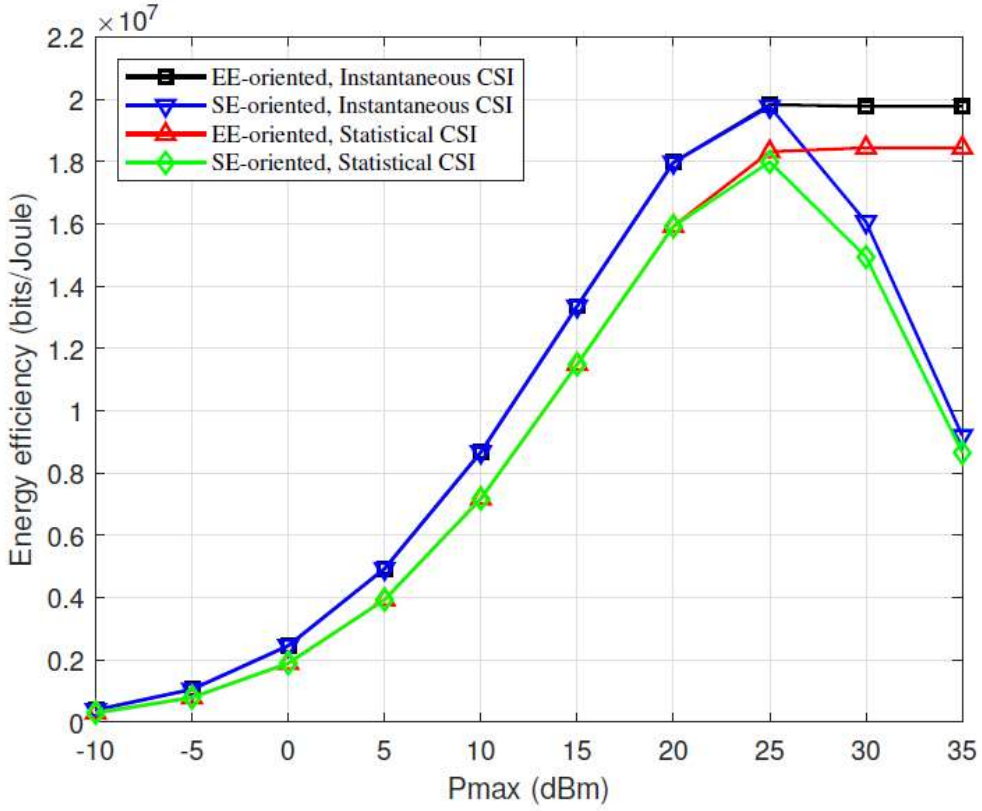

Figure 2-18 EE performance comparison between the instantaneous and statistical CSI cases versus the transmit power budget in both the SE- and EE-oriented approaches.

2.7.6 Conclusion

We studied the EE performance optimization of the DMA-assisted massive MIMO uplink communications, considering both the cases of exploiting the instantaneous as well as statistical CSI. Specifically, we developed a well-structured and low-complexity framework for the transmit covariance design of each user and the DMA configuration strategy at the BS, including the AO and deterministic equivalent methods, as well as Dinkelbach's transform. Based on our algorithm, the DMA-assisted communications achieved much higher EE performance gains compared to the conventional large-scale antenna array-assisted ones, especially in the high power budget region.

2.8 On Maximizing the Sum Secret Key Rate for Reconfigurable Intelligent Surface-Assisted Multiuser Systems

This sub-section summarizes a study that has been detailed in [LSX+22].

2.8.1 Introduction

The channel reciprocity-based key generation (CRKG) method is used for ensuring data confidentiality. Since the CRKG method relies upon the properties of fading channels, it may not guarantee the desired secret key rates in harsh propagation environments. Furthermore, the phenomenon of wave-blockage frequent at high frequency bands leads to an interruption of the communication and the impossibility of generating the secret key. These issues have limited the applicability and scalability of CRKG in wireless networks. Previous works addressed this problem by utilizing a relay node to help forward the received signals between the two key generating parties [ZHL14]. Although a relay may alleviate the problem of secret key generation in harsh propagation environments, it is affected by design challenges. Recently, RIS has been considered as a perfect helper to assist two users in forming an RIS-induced fluctuating channel, which serves as the common randomness for generating secret keys. Till now, only a few works, for example [LLS+21] and [J+21], have considered the problem of optimizing the RIS configuration for the generation of secret keys, however, for the single-user case only. This work aims to address the challenging problem of CRKG between an access point (AP) and multiple users in harsh propagation environments, by capitalizing on the presence of an RIS.

2.8.2 System Model

This study considers an RIS-assisted multiuser key generation system, which comprises a wireless AP (Alice), an RIS, an eavesdropper (Eve) and K legitimate User Terminals (UTs), as shown in Figure 2-19. All parties, including Alice, Eve and the UTs, are assumed to be equipped with a single antenna. Alice intends to generate secret keys $\kappa = \{\kappa_1, \dots, \kappa_K\}$ with the UTs, from the wireless channels between them. A time division duplex (TDD) protocol is assumed. We assume that the direct wireless channels between Alice and the UTs are blocked, therefore an RIS with M elements is deployed to enable the key generation. The phase shifts of the RIS are programmed and reconfigured via a controller.

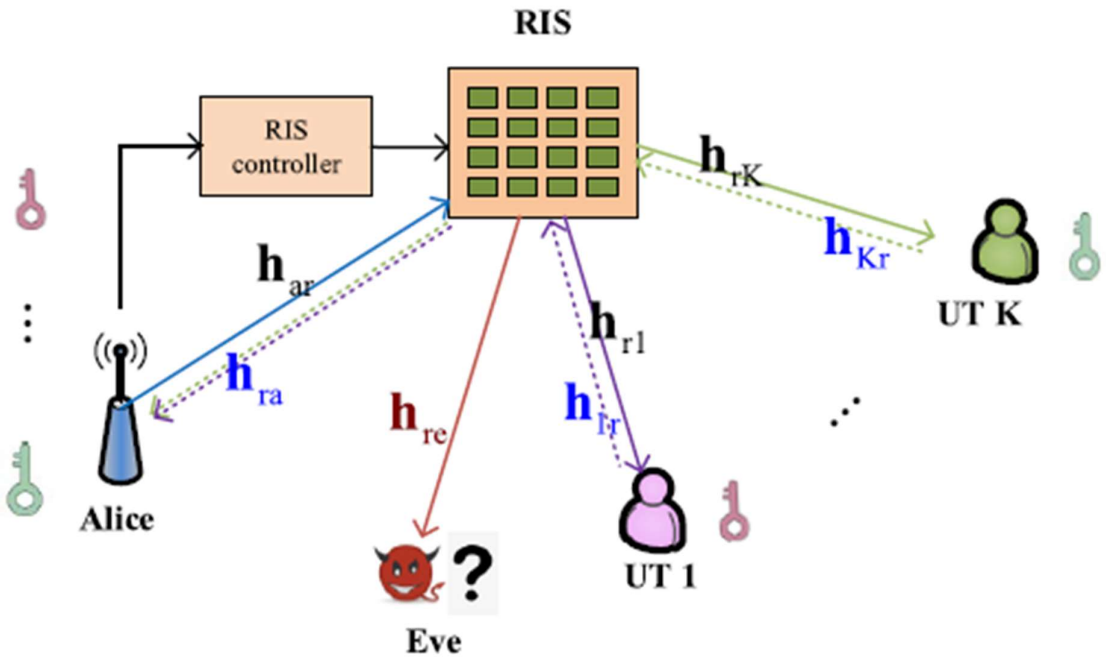

Figure 2-19 System model of an RIS-assisted key generation scheme.

Eve is assumed to be a passive eavesdropper, who pretends to be a legitimate UT and intends to infer the keys in the set $\{\kappa_1, \dots, \kappa_K\}$ based on her own channel observations and the transmissions over the public channel. For simplicity, we define UT k as an arbitrary legitimate UT, while UT k' as the pretending Eve or an arbitrary curious UT.

When the channels of the different UTs and Eve are statistically independent among each other, the secret key rate for the UT k can be simplified to

$$I\left(z_k^{dl}; z_k^{ul}\right) = 2log(1 + \mathrm{v}^H R_k \mathrm{v}) - log(1 + 2\mathrm{v}^H R_k \mathrm{v}) \quad \textbf{(2.8.1)}$$

Where z_k^{dl} $\left(z_k^{ul}\right)$ is the DL (UL) CSI, v is the phase vector and R_k is the correlation matrix.

The optimization target is to find a phase vector v that maximizes the sum secret key rate, as follows

$$\begin{aligned} &\max_{\mathrm{v}} \quad R_{sum}^{c_1} = \textstyle\sum_k I\left(z_k^{dl}; z_k^{ul}\right) \\ &s.t. \quad \mathrm{v}^H E_m \mathrm{v} \le 1 \quad m \in \{1, \dots, N\} \end{aligned} \quad \textbf{(2.8.2)}$$

Where $E_m = e_m e_m^H$, and e_m is the unit-norm vector whose m-th element is 1.
We propose a Lagrange dual algorithm to find a solution $\mathrm{v}_{c_1}^*$, as summarized in Algorithm 1.

Algorithm 1 The Lagrange Dual Algorithm for Solving the Problem in

Require: $\mathbf{R}_1, \mathbf{R}_2, \cdots, \mathbf{R}_K$

Ensure: $\mathbf{v}_{c_1}^*$

1: Initial $\mathbf{v}^{(0)}$ and set $i = 0$ (iteration number).

2: **repeat**

3: Calculate $\tilde{\mathbf{v}}$ as

$$\tilde{\mathbf{v}} = \sum_k \left(1 + (\mathbf{v}^{(i)})^H \mathbf{R}_k \mathbf{v}^{(i)}\right)^{-1} \mathbf{R}_k \mathbf{v}^{(i)} - \sum_k (1 + 2(\mathbf{v}^{(i)})^H \mathbf{R}_k \mathbf{v}^{(i)})^{-1} \mathbf{R}_k \mathbf{v}^{(i)}.$$

4: For every $m \in \{1, 2, \cdots, M\}$, set the Lagrange multipliers $\tilde{\Lambda}_m = |[\tilde{\mathbf{v}}]_m|$ and update $[\mathbf{v}^{(i+1)}]_m$ by

$$[\mathbf{v}^{(i+1)}]_m = \frac{[\tilde{\mathbf{v}}]_m}{\tilde{\Lambda}_m},$$

where $[\cdot]_m$ represents the m-th element in the vector.

5: Set $i = i + 1$ and calculate the sum secret key rate as

$$R^{(i)} = \sum_k I(z_k^{dl}; z_k^{ul}).$$

6: **until** $|R^{(i)} - R^{(i-1)}| \leq \varepsilon$.

When the channels among the different UTs are correlated, the RIS-induced channels are correlated as well. This may cause information leakage among the UTs. To maximize the sum secret key rate, the optimization problem can be expressed as

$$\max_{\mathrm{v}} \quad R_{sum}^{c_2} = \sum_k \min_{k' \neq k} I\left(z_k^{dl}; z_k^{ul} | z_{k'}^{dl}\right) \qquad \textbf{(2.8.3)}$$
$$s.t. \quad \mathrm{v}^H E_m \mathrm{v} \leq 1 \quad m \in \{1, \ldots, N\}$$

Where $I\left(z_k^{dl}; z_k^{ul} | z_{k'}^{dl}\right) = \log \frac{|\hat{R}_{z_k^{dl} z_{k'}^{dl}}| \, |\hat{R}_{z_k^{ul} z_{k'}^{dl}}|}{|\hat{R}_{z_{k'}^{dl}}| \, |\hat{R}_{z_k^{dl} z_k^{ul} z_{k'}^{dl}}|}$, and $\hat{R}$ are the covariance matrices.

Algorithm 2 summarizes the proposed semi-definite relaxation-successive convex approximation (SDR-SCA) based algorithm for solving the problem (2.8.3).

Algorithm 2 The SDR-SCA Based Algorithm for Solving Problem

Require: $\mathbf{R}_1, \mathbf{R}_2, \cdots, \mathbf{R}_K$
Ensure: $\mathbf{v}_{c_2}^*$
1: Initial $\mathbf{V}^{(0)} = \mathbf{v}^{(0)}(\mathbf{v}^{(0)})^H$ and set $i = 0$.
2: **repeat** for the i-th iteration
3: Calculate $x_{k,k'}^{(i)}$ as

$$x_{k,k'}^{(i)} = q_k(\mathbf{V}^{(i)}) + \mathrm{Tr}(\mathbf{R}_{kk'}^H \mathbf{V}^{(i)} \mathbf{R}_{kk'} \mathbf{V}^{(i)}).$$

4: Update $p_k(V, x_{k,k'})$
5: Solve the convex optimization problem
6: Set $i = i + 1$ and calculate the sum secret key rate $(R_{\mathrm{sum}}^{c_2})^{(i)}$.
7: **until** $|(R_{\mathrm{sum}}^{c_2})^{(i)} - (R_{\mathrm{sum}}^{c_2})^{(i-1)}| \leq \varepsilon$.
8: Obtain a rank-1 $\mathbf{V}^*$ by applying the Gaussian randomization method to $\mathbf{V}^{(i)}$.
9: Take the eigenvalue decomposition of $\mathbf{V}^*$ as $\mathbf{V}^* = c\mathbf{u}\mathbf{u}^H$.
10: Obtain $\mathbf{v}_{c_2}^*$ as $\mathbf{v}_{c_2}^* = \sqrt{c}\mathbf{u}$.

2.8.3 Results

The channel from Alice to the RIS and the channel from the RIS to each UT are zero-mean complex Gaussian random variables. Unless otherwise stated, the number of RIS elements is $M = 16$, the number of UTs is $K = 4$, and the signal-to-noise ratio (SNR) is $10\ dB$, where the SNR is defined as the ratio of the transmit power and the noise variance.

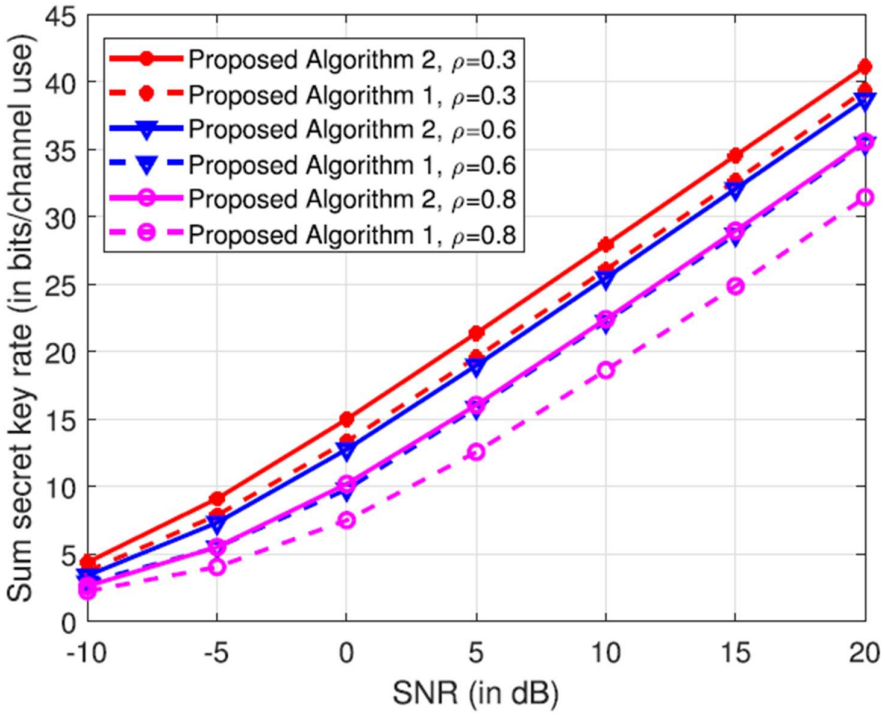

Figure 2-20 Comparison of the sum secret key rates $R_{sum}^{c_2}$ between Algorithm 1 and Algorithm 2 for different channel correlation coefficients.

Figure 2-20 compares the sum secret key rates obtained by using Algorithm 1 and Algorithm 2 as a function of the channel correlation coefficient. The solutions of Algorithm 1 are obtained by optimizing the RIS configuration under the assumption of independent channels. Therefore, when these solutions are substituted into the expression of $R_{sum}^{c_2}$, their rates are greatly reduced. As expected, Algorithm 2 outperforms Algorithm 1 in the considered SNR range. In particular, the sum secret key rate gain becomes more distinct, when the channel correlation coefficient increases from 0.3 to 0.8. Figure 2-20 confirms that the sum secret rate can be enhanced if the channel correlation among the UTs is taken into account at the design stage.

2.8.4 Conclusion

In this work, we introduced a multiuser secret key generation scheme that capitalizes on the presence of RISs in the environment. The RIS-induced channel model was modelled as the sum-of-product of the channel from Alice to the RIS, the phase shifts applied by the RIS, and the channel from the RIS to the UT. Based on this channel model, a general closed form expression of the secret key rate was derived. In order to achieve the maximum sum secret key rate, we formulated and solved an optimization problem to obtain the optimal RIS configuration over independent and correlated channels among the UTs. Over independent channels, a Lagrange dual algorithm was proposed for optimizing the phase shifts of the RIS elements. Over correlated channels, on the other hand, we proposed an SDR-SCA based algorithm. Numerical results demonstrated that the proposed scheme provides the highest sum secret key rate as compared with existing benchmark schemes. Therefore, the proposed scheme boosts the SSE.

3 Assessment methods of EE, EMFEU and SSE Improvements

This section summarizes the work performed within Task 6.3. For each of the various new models to assess EE, SSE or EMFEU that were proposed by WP6, Task 6.3, the following brief description is provided:

- Objective.
- System model.
- Initial performance results (if available).
- Conclusion.

Note that for more mature models, the detailed description of the proposed models and their performance is available in submitted/accepted papers. For other schemes, at an earlier stage of study, only initial views on expected performance are provided. For those latter schemes, finalized results will be provided in the upcoming deliverable D6.3.

3.1 Battery recharging time models for reconfigurable intelligent surfaces-assisted wireless power transfer systems

This section summarizes a study that is to appear in [MMA+22].

3.1.1 Introduction

Wireless power transfer (WPT) has been highly recognized in both academia and industry as a promising technology to address the energy sustainability problem of wireless nodes and has rapidly gained a growing interest in the research of B5G communication networks. [WZ20] [P+20][WZ19] assume battery free RF energy harvesting (RFEH) energy receivers (ERs), whose harvested energy is directly used for future transmissions. In this case, the amount of the received RF signals, and consequently, the amount of harvested energy, is considered to be sufficient and predictable over a certain period of time. However, in scenarios where RFEH nodes are equipped with batteries [AK14], the harvested energy is stored first in the battery before being used for future transmissions. Since the power of the received RF signal depends on the distribution of the probabilistic wireless fading channel between the transmitter and the receiver, the RFEH process and similarly, the time required to recharge the battery of an RFEH node, called the battery recharging time (BRT), become stochastic processes. To the best of our knowledge, the statistical characterization of BRT is not yet studied in the open literature. Motivated by this, the prime focus of this work is to develop a novel theoretical framework to characterize the statistical properties of BRT for RIS-assisted WPT systems, consisting of ERs with limited battery capacity.

3.1.2 System Model

In this paper, we consider a single-antenna RF source node, S, and a single-antenna energy-constrained ER, as depicted in Figure 3-1. The ER could be a low-power sensor node equipped with a battery with a finite capacity. In order to extend the operational range of the ER, while ensuring that its harvested energy is sufficient for real-life operation, we propose WPT assisted by an RIS. The end-to-end (E2E) channel gain between S and ER characterizes the power received at the ER, and accordingly, defines the behavior of the overall RFEH process, including the instantaneous BRT at ER.

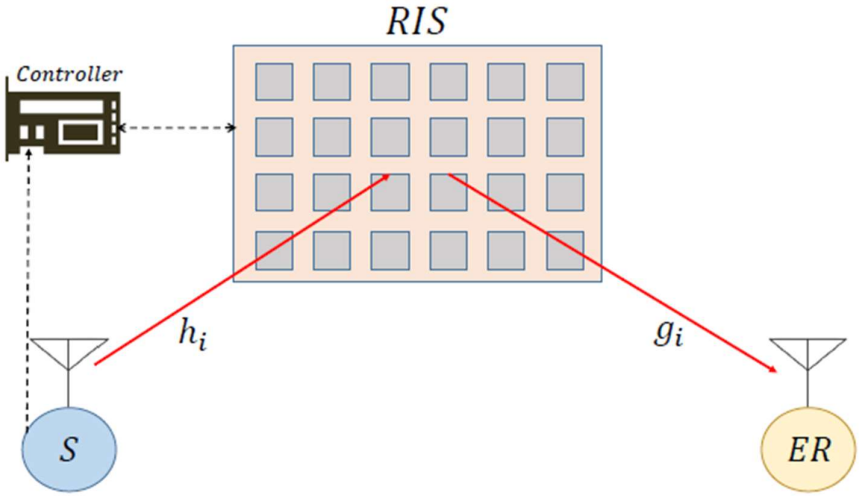

Figure 3-1 RIS-assisted WPT system model

We further assume that a direct link does not exist between S and ER, WPT can be achieved only via the RIS. In our setup, we consider an RIS of N reflecting elements (REs). Each of the elements can be reconfigured by a communication-oriented software through a controller. The power transmitted from S, being either a BS or an RF source, which is reflected by the RIS towards the ER, is harvested and stored in a battery with a limited capacity before being used in future signal transmissions. h_i and g_i denote the small scale complex channel fading coefficients of the $S \rightarrow$ RIS and RIS $\rightarrow$ ER links, respectively, where $|h_i|, |g_i| \sim \mathcal{CN}(0,2\sigma^2)$ for $i \in \{1, \dots, N\}$.

Let P_s denote the transmit wireless power of the source node. The instantaneous total power received at ER through the i-th element of RIS is expressed as

$$P_r = \frac{P_s}{d_1^{\delta} d_2^{\delta}} B^2 \quad \textbf{(3.1.1)}$$

where $B = \sum_{i=1}^{N} |h_i||g_i|$ is the E2E channel gain, d_1 and d_2 represent the distance between S and the center of the RIS and between the center of the RIS and ER, δ is the path loss exponent.

As previously mentioned, the BRT, T_r, is determined by the amount of power received and then harvested at ER

$$T_r = \frac{\alpha}{P_r} \quad \textbf{(3.1.2)}$$

where α is the conversion coefficient, which is a function of the battery and the RFEH circuit parameters.

For RIS-assisted WPT systems, the PDF of the battery recharging time at ER node is given as

$$f_{T_r}(\tau) \approx \frac{a_1 a_2}{2\tau} G_{1,2}^{2,0}\left[\frac{1}{a_2}\sqrt{\frac{\alpha}{\bar{P}_r \tau}}\middle|_{a_5+1, a_4+1; -}^{-; a_3+1}\right], \quad \tau > 0 \quad \textbf{(3.1.3)}$$

We obtain the CDF of the BRT in a closed-form as

$$F_{T_r}(\tau_{th}) = 1 - a_1 a_2 G_{2,3}^{2,1}\left[\frac{1}{a_2}\sqrt{\frac{\alpha}{\bar{P}_r \tau_{th}}}\middle|_{a_4+1, a_5+1; 0}^{1; a_3+1}\right], \quad \tau_{th} > 0 \quad \textbf{(3.1.4)}$$

$$a_1 = \frac{\Gamma(a_3 + 1)}{a_2 \Gamma(a_4 + 1)\Gamma(a_5 + 1)}$$

$$a_3 = \frac{4\varphi_4 - 9\varphi_3 + 6\varphi_2 - \mu_1}{-\varphi_4 + 3\varphi_3 - 3\varphi_2 + \mu_1}$$

$$a_2 = \frac{a_3}{2}(\varphi_4 - 2\varphi_3 + \varphi_2) + 2\varphi_4 - 3\varphi_3 + \varphi_2$$

$$a_4 = \frac{a_6 + a_7}{2}$$

$$a_5 = \frac{a_6 - a_7}{2}$$

$$a_6 = \frac{a_3(\varphi_2 - \mu_1) + 2\varphi_2 - \mu_1}{a_2} - 3$$

$$a_7 = \sqrt{\left(\frac{a_3(\varphi_2 - \mu_1) + 2\varphi_2 - \mu_1}{a_2} - 1\right)^2 - 4\,\frac{\mu_1(a_3 + 1)}{a_2}}$$

$$\varphi_i = \frac{\mu_j}{\mu_{j-1}}, j > 1$$

$$\overline{P_r} = \frac{P_r}{d_1^{\delta} d_2^{\delta}}$$

Where $G_{\cdot,\cdot}^{\cdot,\cdot}[.|.]$ denotes the Meijer G-function, μ_j is the j-th moment of B and Γ is the gamma function.

The n-th order moment of the BRT, denoted by $\mu_{T_r}(n)$, is a very useful statistical tool, as it enables the characterization of the mean value of the BRT, in addition to other underlying useful properties such as its skewness and kurtosis.

$$\mu_{T_r}(n) = a_1 a_2^{(1-2n)} \left(\frac{\alpha}{\overline{P_r}}\right)^n \frac{\Gamma(a_4 + 1 - 2n)\,\Gamma(a_5 + 1 - 2n)}{\Gamma(a_3 + 1 - 2n)} \quad \textbf{(3.1.5)}$$

The mean value of the BRT when $N > 1$ converges to

$$\overline{T_r} = E[\tau_r] = \frac{4\alpha}{(N^2\pi^2 + N(16 - \pi^2))\overline{P_r}} \quad \textbf{(3.1.6)}$$

3.1.3 Results

In this section, numerical and Monte Carlo simulation results are presented to validate the accuracy of the proposed theoretical framework. This section also focuses on characterizing the properties of the BRT in RIS-assisted WPT wireless systems. The term Monte Carlo simulations refers to the use of actual fading channel variates with a number of repetitions of 10^6 trials. Unless otherwise stated, the RFEH efficiency factor $\eta = 0.5$, as a worst case scenario, capturing the effects of low-cost hardware, and the total distance, d_{tot}, between the source node, S, and the ER node is set to $5\ m$. In order to ensure far-field WPT, we assume that the size of RIS is relatively smaller than the transmission distance. It is assumed that the RIS is located mid-way between S and ER, i.e., $d_1 = d_2 = d_{tot}/2$, and the path-loss exponent, $\delta = 2.7$. Also, it is recalled that P_s defines the total transmit power of the system.

To gain more insights about the effect of varying the transmit power on the statistical distribution of the BRT in RIS-assisted WPT systems, we provide in Figure 3-2 the CDF as a function of the BRT threshold, T_r, of the RIS-assisted system. The examination is carried out for different N

values and assuming two transmit power scenarios, namely low- ($P_s = 7\ dBm$) and high- ($P_s = 30\ dBm$) transmit power. The excellent fit between the simulation and the analytical results verifies the accuracy of our developed theoretical framework. As expected, for a fixed N, as the T_r increases, the CDF value increases. Additionally, for a given T_r value, as N increases, the CDF value improves. This indicates that the efficiency of the RFEH process is remarkably improved in an RIS-assisted WPT system by increasing the number of REs, N.

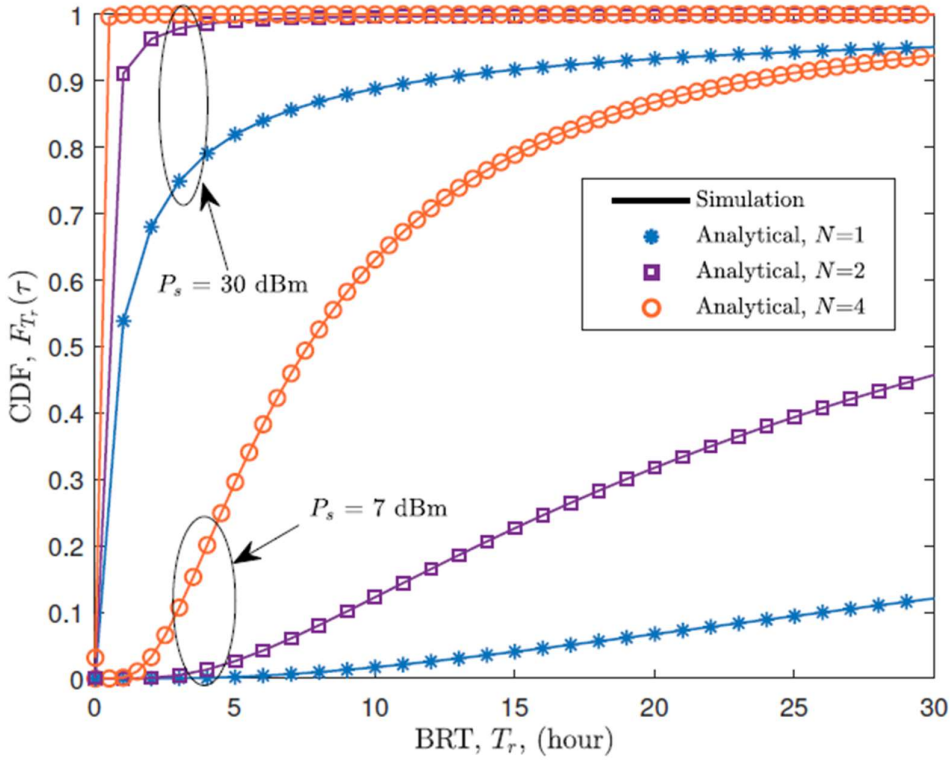

Figure 3-2 The CDF as a function of BRT threshold for RIS-assisted for low- and high- transmit power scenarios and for different values of N

3.1.4 Conclusion

In this work, we developed a theoretical framework to investigate the energy sustainability of RIS-assisted WPT systems, from the BRT perspective of an RFEH node. We derived novel low complexity tight closed-form approximations for the PDF, CDF, and moments of the BRT as functions of the received power, battery parameters, and number of RIS REs. Besides being accurate and mathematically tractable, our results reveal that the proposed statistical tools provide an efficient means to evaluate RIS-assisted WPT systems and extract useful design insights. For example, our results show that doubling the number of RIS elements improves the predictability of the BRT of the RFEH nodes in the network and offers a 4-fold reduction in its mean value. Moreover, it is reported that the characteristics of the BRT are significantly impacted not only by the system parameters, such as the distance between the nodes, but also by the battery parameters of the RFEH node, such as the battery capacity. Finally, our results illustrated that significant performance gains in the BRT have been observed by locating the RIS close to the source or to the RFEH node.

3.2 Development of modelling tools by FDTD methods, and integration with framework provided by WP3.

3.2.1 Introduction

In WP3 the modelling activity focused on considering a metasurface, called RIS in our case, by adopting the generalized sheet transition conditions (GSTCs) method. This method makes use of a particular set of boundary conditions (BCs) that takes into account discontinuities for the tangential **E** and **H** fields introduced by the insertion of the metasurface within the simulation domain. The RIS is a very complex structure which is composed by many subwavelength particles like unit cells, arbitrarily shaped or not. In order to overcome the physical complexity of the simulation problem, the RIS has been modelled as a homogeneous sheet consisting of a subwavelength thickness, as depicted in Figure 3-3. In this way, the overall characterization of the RIS behaviour is greatly simplified and a continuous mathematical treatment can be used, in particular by using a continuous tensorial susceptibility function $\bar{\bar{\chi}}(x,y)$. The design and evaluation of the RIS can be done by interchanging two operations: synthesis and analysis. In the first case, given a certain wave transformation operated by the RIS, we derive the parameters of the susceptibility function. In the second case, given the parameters of the susceptibility function we can observe and evaluate the wave transformation operated by the RIS [HKG+21][VCA+18].

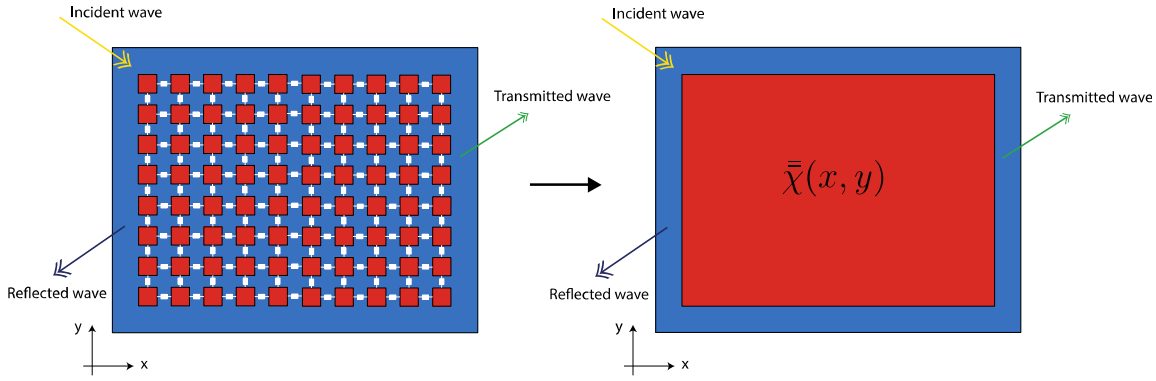

Figure 3-3 RIS

3.2.2 System Model

In RISE-6G, CNIT (Ancona) partner have developed a homemade FDTD code over the last 30 years [MBM16]. This code allows us to simulate a 3D large complex structure. The aim of this cross-collaboration with WP3 is to integrate RISs in this existing code in order to simulate and evaluate the RISs functionalities such as wave transformation, e.g., reflection, focusing on a desired target and so on. To this purpose, the conventional FDTD equations for the **E** and **H** fields have to be updated considering the RIS insertion [VCA+18] [JYL+20]. In those equations, the values of the surface susceptibility are also added.
Basically, the GSTCs generalized the BCs and include the surface material polarization.
$\mathbf{P_s}$ and $\mathbf{M_s}$ are the electric and magnetic polarization densities, as follows:

$$\overrightarrow{P_s} = \epsilon_0 \bar{\bar{\chi}}_{ee} \vec{E}_{av} + \bar{\chi}_{em} \sqrt{\epsilon_0 \mu_0} \vec{H}_{av}$$

$$\overrightarrow{M_s} = \overline{\chi}_{me}\sqrt{\frac{\epsilon_0}{\mu_0}}\vec{E}_{av} + \overline{\overline{\chi}}_{mm}\vec{H}_{av}$$

where the subscript “av”, referred to the electric and magnetic fields, denotes the average fields at both sides of the RIS, $\overline{\chi}_{ee}, \overline{\chi}_{mm}, \overline{\chi}_{em}, \overline{\chi}_{me}$
are the electric and magnetic susceptibility tensors that express the response to the electric and magnetic excitation, ϵ_0 and μ_0 denote the free space permittivity and permeability respectively, whereas the susceptibility tensor is read as follows:

$$\begin{pmatrix} \chi_{ab}^{xx} & \chi_{ab}^{xy} & \chi_{ab}^{xz} \\ \chi_{ab}^{yx} & \chi_{ab}^{yy} & \chi_{ab}^{yz} \\ \chi_{ab}^{zx} & \chi_{ab}^{zy} & \chi_{ab}^{zz} \end{pmatrix}$$

where subscripts “ab” indicates the cases (e,e), (e,m), (m,e) and (m,m).

The whole susceptibility tensor model has 36 components; thus, it is impossible to solve this system directly. To simplify the problem and reduce the susceptibility tensor, it is possible to fix some assumptions without loss of generality, considering properties such as reciprocity, loss, and passivity.

3.2.3 Conclusion

The GSTCs model permits us to easily simulate and handle RISs within the FDTD code considering a continuous and homogeneous sheet with respect considering local fields on a metasurface that consists of microscopic unit cells, with different behaviour each other.
We are developing the FDTD code integrating RISs, and next steps are related to evaluate the stability of the method and to synthetize the susceptibility tensor in order to get the desired behaviour of the RISs.

3.3 Power balance model for RIS-assisted RC (Method for estimating the average EMFEU in complex scattering environments

This section summarizes and extends a work that is partly detailed in the [DVR+22] to include the multipath fading as emulated in reverberating environments.

3.3.1 Introduction

The system that we consider is an end-to-end wireless communication system operating within an RIS-assisted confined environment, e.g., the smart factory or the train station considered for the RISE-6g field trial. While EMF enhancement metrics have been defined in RIS-assisted wireless links in free-space, multiple wave reflections due to walls and objects within the propagation environment must be modelled self-consistently. A natural starting point for including the back-reaction of the environment into the RIS re-radiation resides in assuming the presence of Rician multi-path fading impinging onto the RIS. More precisely, the estimation of the EMFEU in RIS-assisted wireless systems operating within complex scattering environments is tackled by adopting the electromagnetic RC, an echoic chamber that generates controlled multi-path fading in the laboratory [MP+20]. It has been shown in Section 3.2 that the RC is a large, shielded room operated as an over-moded metallic enclosure, and therefore can emulate both indoor as well as urban outdoor environments by adjusting amount and type of absorbing material that degrades the quality factor of the metallic cavity. The cavity interior is mostly empty to host the device under test and includes an irregular metallic structure – the mechanical mode stirrer – that breaks the geometrical symmetry of the room. We follow the nomenclature adopted in previous reports that users generating and perceiving undesired radiation are classified as *non-intended* (*NI*) users, while users generating and perceiving desired radiation are considered as *intended* (*I*) users. The scenario that we analyse is depicted in Figure 3-4, where a 5G BS illuminates both an *I*- and *NI*-user through the RIS in free-space (Figure 3-4 (a)) and within a confined environment (Figure 3-4 (b)). Note that confined environment includes objects that both scatter and absorb the interior cavity energy. Furthermore, it is assumed that no LOS channels are present between BS and users due to blockage. The fundamental mechanism that distinguishes a confined environment from a free-space environment is the re-injection of waves with the environments: this process is underpinned by multi-path fading and reaches the equilibrium after a short (few μs) early-time transient through the competition between RIS re-radiation and environment re-injection. A statistical model is developed that describes the average EM power within the RIS-assisted RC at equilibrium.

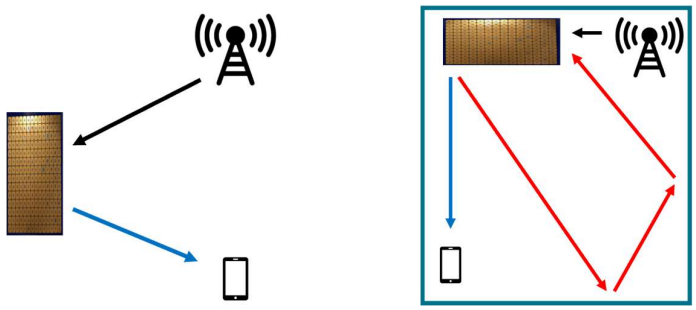

(a) (b)

Figure 3-4 RIS-assisted wireless link (a) in free-space, and (b) in confined environment.

3.3.2 System Model

We developed a model based on laboratory facilities at CNIT (Ancona unit), Italy, where a live 5G base station, connected with the national TI mobile network, operates inside a large-scale RC. Whilst the 5G base station provides the excitation source injecting EM energy inside the RC, selected UE devices receive the digital signal carrying digital information. We focus on narrowband operation of the RC even though the base station can produce real-life signal with broad spectral content. The RC supports wireless signal propagation by confinement and a large fraction of the energy is dissipated within walls, apertures, and absorbing material present in the cavity interior. While this appears as an overly inefficient process for the SISO system, we remark that the absorbing mechanism emulates the path-loss underpinned by (unintended) objects and users nearby the (intended) wireless link. We first consider as a target service, a DL data communication towards an *I*-UE. We also consider an (unlocalized) *NI* user/person/object who is potentially exposed to the EMF generated in DL. Referring to Figure 3-4 (a), the average power received by the RIS reads

$$\boldsymbol{P_{RIS}(\Omega_d) = \alpha(d)\, g_{RIS}(\Omega_d)\, g_T(\Omega_d)\, P_T} \quad \textbf{(3.3.1)}$$

where $\boldsymbol{P_T}$ is the input power, $\boldsymbol{g_T}$ and $\boldsymbol{g_{RIS}}$ are the antenna gain of the base station and the antenna gain of the RIS, respectively, along the LOS channel at angle $\boldsymbol{\Omega_d}$, and $\boldsymbol{\alpha(d)}$ is the free-space path loss at distance $\boldsymbol{d}$ from the base station. Similarly, and assuming blockage between base station and *I*-user, the average power received by the kth UE terminal through the RIS reads

$$\boldsymbol{P_{R,k}\,(\Omega_D) = \alpha(D)\, g_{R,k}(\Omega_D)\, \langle p_m \rangle(\Omega_D)} \quad \textbf{(3.3.2)}$$

with $\boldsymbol{g_{R,k}(\Omega_D)}$ gain of the UE antenna along the LOS channel at angle $\boldsymbol{\Omega_D}$, and free-space path loss defined as

$$\boldsymbol{\alpha(l) = \left(\frac{\lambda}{4\pi l}\right)^2} \quad \textbf{(3.3.3)}$$

The calculation of $\boldsymbol{\langle p_m \rangle(\Omega_D)}$ is a delicate task that ensures self-consistency between RC re-injected power and RIS re-radiation. Following the scheme in Figure 3-4 (b) we note that the power re-radiated by the RIS depends on both the direct illumination from the base station and the RC power re-injected in the environment

$$\boldsymbol{p_m(\Omega_D) = g_{RIS}(\Omega_D)\, m(\Omega_d)\, P_{RIS}(\Omega_d) + g_{RIS}(\Omega_D)\, m(\Omega)\, P_{RC}(\Omega)} \quad \textbf{(3.3.4)}$$

with incident angle $\boldsymbol{\Omega_i}$, $\boldsymbol{m(\Omega)}$ RIS re-radiation efficiency towards $\boldsymbol{\Omega}$ [DVR+22], and $\boldsymbol{P_{RC}(\Omega)}$ power re-injected by the RC and captured by the RIS at angle $\boldsymbol{\Omega}$. Considering a large RIS

$$\boldsymbol{P_{RC}(\Omega) = A_{RIS}(\Omega)\, S_{RC}} \quad \textbf{(3.3.5)}$$

where $\boldsymbol{A_{RIS}(\Omega)}$ is the effective RIS geometrical area seen at angle $\boldsymbol{\Omega}$, and $\boldsymbol{S_{RC}}$ is the average (isotropic and homogeneous) cavity power density at equilibrium within the RC. Furthermore, the average power re-radiated by the RIS towards the UE terminal is obtained from the average through the multi-path rays re-injected at angle $\boldsymbol{\Omega}$

$$\boldsymbol{\langle p_m \rangle(\Omega_D) = \int p_m(\Omega, \Omega_D)\, dp_m(\Omega)} \quad \textbf{(3.3.6)}$$

Finally, inserting (3.3.1) and (3.3.4) in (3.3.6) yields an expression for $\boldsymbol{P_{RC}(\Omega)}$ that is needed to calculate $\boldsymbol{P_{R,k}}$ in (3.3.2). In particular, $\boldsymbol{P_{RC}(\Omega)}$ is obtained by the power balance equation [PM10]

$$\boldsymbol{P_0 + P_{R,k} - P_T = 0} \tag{3.3.7}$$

where $\boldsymbol{P_0}$ is the power transmitted inside the RC, which is obtained by removing the power carried by the virtual LOS from the power radiated by the source. From above, we unfold the linear relation between $\boldsymbol{P_{R,k}}$ and $\boldsymbol{P_{RC}(\Omega)}$, while P_0 and $P_{RC}(\Omega)$ are related by the average RC quality factor, viz.,

$$\boldsymbol{\frac{16\,\pi^2\,V}{\lambda^3\,Q}\,\langle P_{RC}\rangle = P_T - P_{R,k}} \tag{3.3.8}$$

The power balance model leads to an angle dependent expression of the average received power $\boldsymbol{\langle P_{RC}\rangle(\Omega_D)}$ which leads to an angle dependent, and thus an (anisotropic) Rice $\boldsymbol{\mathcal{K}}$-factor $\boldsymbol{\mathcal{K} = \frac{P_{R,k}\,(\Omega_D)}{\langle P_{RC}\rangle(\Omega_D)}}$. The model achieved in this study constitutes the basis to devise the average SNR – and the average data-rate $\boldsymbol{R^{DL}}$ that is needed in the definition of **inter-EMFEU**. Inherently, $\boldsymbol{\langle P_{RC}\rangle}$ can be used as an estimate of the power stressing onto an NI user/object $\boldsymbol{X^{NI}}$. This approximation is valid if the user/object does not absorb RC power. A better approximation can be devised by considering the presence of both the users in the power balance equations (3.3.8) and (3.3.9). The power balance approach can be extended to multi-user scenarios. A similar reasoning can be applied to UL and arrive at an estimate of the average **self-EMFEU.**

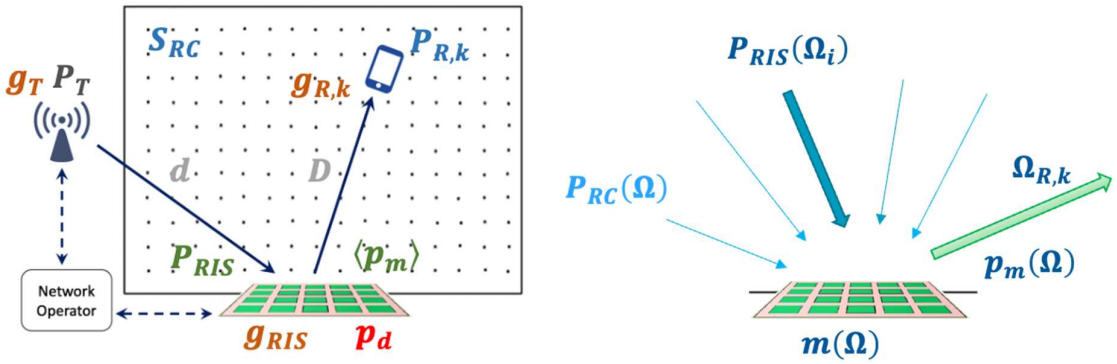

(a) (b)

Figure 3-5 System Model of a SISO system operating in a RIS-assisted RC in DL.

3.3.3 Conclusion

We have developed an anisotropic power balance model for RIS-assisted reverberation chambers. The model constitutes the basis for the estimation of average EMFEU metrics in complex rich scattering electromagnetic environments and can be extended to multi-user and multi-RIS operation. The model stands on the re-radiation theory of RISs, which introduces a reflection coefficient for the anomalous RIS radiation modes. Inherently, the gain $\boldsymbol{g_{RIS}(\Omega_d)}$ is proportional to the effective area of the RIS aperture in large RISs. Next steps include optimizing the RIS re-radiation factor $\boldsymbol{m(\Omega_d)}$ upon maximization/minimization of (3.3.2).

4 Conclusions

In this deliverable, we summarize the intermediate results of Task 6.2 on Sustainable RIS Solutions Design for EE, EMFEU and SSE and Task 6.3 on assessment methods of EE, EMFEU and SSE Improvements.
We present eight solutions and innovations to boost the EE, EMFEU or SSE metrics and three new models to assess these metrics. Final results will be provided in the upcoming deliverable D6.3.

5 References

[ACS22]	F. Ezzahra. Airod, M. Merluzzi, A. Clemente, E. Calvanese Strinati, “Blue Communications for Edge Computing: the Reconfigurable Intelligent Surfaces Opportunity”, submitted to Globecom 2022.
[AK14]	D. Altinel and G. K. Kurt, “Statistical models for battery recharging time in RF energy harvesting systems,” in Proc. IEEE Wireless Commun. Netw. Conf. (WCNC), 2014, pp. 636–641.
[APV21]	N. Awarkeh, D. -T. Phan-Huy and R. Visoz, "Electro-Magnetic Field (EMF) aware beamforming assisted by Reconfigurable Intelligent Surfaces," 2021 IEEE 22nd International Workshop on Signal Processing Advances in Wireless Communications (SPAWC), 2021, pp. 541-545.
[APV+22-1]	N. Awarkeh, D.-T. Phan-Huy, R. Visoz, M. di Renzo "A Novel RIS-Aided EMF-Aware Beamforming Using Directional Spreading, Truncation and Boosting," accepted to EuCNC 2022.
[APV+22-2]	N. Awarkeh, D.-T. Phan-Huy, R. Visoz, M. di Renzo "A Novel RIS-Aided EMF Exposure Aware Approach using an Angularly Equalized Virtual Propagation Channel," accepted to EuCNC 2022.
[BRR+19]	Basar, M. D. Renzo, J. De Rosny, M. Debbah, M.S. Alouini and R. Zhang, “Wireless Communications through Reconfigurable Intelligent Surfaces,” IEEE Access, vol. 7, pp. 116753-116773, 2019.
[C+19]	Colombi et al., “Assessment of Actual Maximum RF EMF Exposure from Radio Base Stations with Massive MIMO Antennas,” PhotonIcs \& Electromagnetics Research Symp. - Spring, pp. 570-577, June 2019.
[C+21]	M. R. Castellano et al., “Dynamic electromagnetic exposure allocation for Rayleigh fading MIMO channels,” IEEE Trans. Wireless Commun., vol. 20, no. 2, pp. 728–740, Feb. 2021.
[CEA21]	L. Chiaraviglio, A. Elzanaty and M. -S. Alouini “Health Risks Associated With 5G Exposure: A View From the Communications Engineering Perspective,” in IEEE Open Journal of the Communications Society, vol. 2, pp. 2131-2179, 2021.
[CLS+12]	A. Clemente, L. Dussopt, R. Sauleau, P. Potier and P. Pouliguen, ”Focal Distance Reduction of Transmit-Array Antennas Using Multiple Feeds,” in IEEE Antennas and Wireless Propagation Letters, vol. 11, pp. 1311-1314, 2012, doi: 10.1109/LAWP.2012.2227105.
[DTT16]	E. Degirmenci, B. Thors and C. Tornevik, “Assessment of Compliance With RF EMF Exposure Limits: Approximate Methods for Radio Base Station Products Utilizing Array Antennas With Beam-Forming Capabilities,” IEEE Transactions on Electromagnetic Compatibility, vol. 58, no. 4, pp. 1110-1117, August 2016.
[DVR+22]	V. Degli-Esposti, E. M. Vitucci, M. Di Renzo and S. Tretyakov, "Reradiation and Scattering from a Reconfigurable Intelligent Surface: A General Macroscopic Model," in IEEE Transactions on Antennas and Propagation, doi: 10.1109/TAP.2022.3149660.
[GS+22]	H. Guo and T. Svensson, "Electromagnetic Field Exposure Perspective in Reconfigurable Intelligent Surface-Assisted Networks: Challenge or Chance," under preparation, 2022.
[HKG+21]	C. L. Holloway, E., F. Kuester, J. A. Gordon, J. O’Hara, J. Booth and D. R. Smith, “An overview of the theory and applications of metasurfaces: The two dimensional equivalents of metamaterials”, IEEE Antennas Propag. Mag., vol54, no. 2, pp. 10-35, Apr. 2021.

[ICN20]	"ICNIRP guidelines for limiting exposure to electromagnetic fields (100 kHz – 300 GHz)," https://www.icnirp.org/cms/upload/publications/ICNIRPrfgdl2020.pdf
[IEA+22]	H. Ibraiwish, A. Elzanaty, Y. Al-Baderneh, and M. Alouini, "EMF-aware cellular networks in RIS-assisted environments," IEEE Communications Letters, vol. 26, no. 1, pp. 123–127, 2022.
[J+21]	Z. Ji et al., "Secret key generation for intelligent reflecting surface assisted wireless communication networks," IEEE Trans. Veh. Technol., vol. 70, no. 1, pp. 1030–1034, Jan. 2021.
[JYL+20]	X. Jia, F. Yang, X. Liu, M. Li and S. Xu, "Fast Nonuniform Metasurface Analysis in FDTD Using Surface Susceptibility Model," IEEE Transactions on Antennas and Propagation, vol. 68, no. 10, pp. 7121-7130, Oct. 2020.
[L99]	T. K. Y. Lo, "Maximum Ratio Transmission," IEEE Transactions on Communications, vol. 47, no. 10, pp. 1458-1461, Oct. 1999.
[LLS+21]	X. Lu, J. Lei, Y. Shi, and W. Li, "Intelligent reflecting surface assisted secret key generation," IEEE Signal Process. Lett., vol. 28, pp. 1036–1040, 2021.
[LSX+22]	G. Li, C. Sun, W. Xu, M. D. Renzo and A. Hu, "On Maximizing the Sum Secret Key Rate for Reconfigurable Intelligent Surface-Assisted Multiuser Systems," in IEEE Transactions on Information Forensics and Security, vol. 17, pp. 211-225, 2022, ttps://hal-centralesupelec.archives-ouvertes.fr/hal-03506039 .
[MBM16]	F. Moglie, L. Bastianelli, and V. Mariani Primiani. "Reliable finite- difference time-domain simulations of reverberation chambers by using equivalent volumetric losses," IEEE Trans. Electromagnetic Compatibility, vol. 58, no. 3, pp. 653–660, Jun. 2016.
[MHM+18]	Morgado, K. M. S. Huq, S. Mumtaz and J. Rodriguez, "A Survey of 5G Technologies: Regulatory, Standardization and Industrial Perspectives," Digital Comm. and Net., no. 4, pp. 87-97, 2018.
[MMA+22]	Lina Mohjazi, Sami Muhaidat, Qammer H. Abbasi, Muhammad Ali Imran, Octavia A. Dobre, Marco Di Renzo "Battery recharging time models for reconfigurable intelligent surfaces-assisted wireless power transfer systems," IEEE Transactions on Green Communications and Networking, 2022 (to appear). https://arxiv.org/abs/2007.05227
[MP+20]	V. M. Primiani et al., "Reverberation chambers for testing wireless devices and systems," in IEEE Electromagnetic Compatibility Magazine, vol. 9, no. 2, pp. 45-55, 2nd Quarter 2020, doi: 10.1109/MEMC.2020.9133241.
[P+20]	C. Pan et al., "Intelligent reflecting surface aided MIMO broadcasting for simultaneous wireless information and power transfer," IEEE J. Sel. Areas Commun., 2020.
[PCE+18]	S. Persia, C. Carciofi, S. D'Elia and R. Suman, "EMF Evaluations for Future Networks based on Massive MIMO," Int'l Symp. on Personal, Indoor and Mobile Radio Comm. (PIMRC), pp. 1197-1202, Sept. 2018.
[PM10]	Primiani, V.M. and Moglie, F., 2010. "Numerical simulation of LOS and NLOS conditions for an antenna inside a reverberation chamber. Journal of Electromagnetic Waves and Applications," 24(17-18), pp.2319-2331.
[R+13]	F. Rusek et al., "Scaling up MIMO: Opportunities and Challenges with Very Large Arrays," IEEE Sig. Proc. Mag., vol. 30, no. 1, pp. 40-60, Jan. 2013.
[R+19]	M. D. Renzo, et al. "Smart Radio Environments Empowered by Reconfigurable AI Meta-Surfaces: an Idea whose Time has Come," EURASIP J. on Wireless Comm. and Net., May 2019.
[R+21-1]	R. Fara et al., "Reconfigurable Intelligent Surface-Assisted Ambient Backscatter Communications – Experimental Assessment," 2021 IEEE ICC Workshops, 2021, pp. 1-7.

[R+21-2]	R. Fara et al., "A Prototype of Reconfigurable Intelligent Surface with Continuous Control of the Reflection Phase," in IEEE Wireless Communications, vol. 29, no. 1, pp. 70-77, February 2022.
[RH10]	Randy L. Haupt, "Antenna Arrays: A Computational Approach," Wiley-IEEE Press, 2010
[S+21]	C. Strinati et al., "Wireless Environment as a Service Enabled by Reconfigurable Intelligent Surfaces: The RISE-6G Perspective," 2021 Joint EuCNC/6G Summit, 2021, pp. 562-567.
[SAI+21]	N. Shlezinger, G. C. Alexandropoulos, M. F. Imani, Y. C. Eldar, and D. R. Smith, "Dynamic metasurface antennas for 6G extreme massive MIMO communications," IEEE Wireless Commun., vol. 28, no. 2, pp. 106–113, Apr. 2021.
[SDE+19]	N. Shlezinger, O. Dicker, Y. C. Eldar, I. Yoo, M. F. Imani, and D. R. Smith, "Dynamic metasurface antennas for uplink massive MIMO systems," IEEE Trans. Commun., vol. 67, no. 10, pp. 6829–6843, Oct. 2019.
[TFC+17]	Thors, A. Furuskär, D. Colombi and C. Tornevik "Time-Averaged Realistic Maximum Power Levels for the Assessment of Radio Frequency Exposure for 5G Radio Base Stations Using Massive MIMO,"' IEEE Access, vol. 5, pp. 19711-19719, Sept. 2017.
[TP16]	F. Talebi and T. Pratt, "Channel Sounding and Parameter Estimation for a Wideband Correlation-Based MIMO Model," IEEE Trans. on Vehicular Technology, Vol. 65, no. 2, Feb. 2016.
[VAT18]	E. Vlachos, G. C. Alexandropoulos, and J. Thompson, "Massive MIMO channel estimation for millimeter wave systems via matrix completion," IEEE Signal Process. Lett., vol. 25, no. 11, pp. 1675–1679, Nov. 2018.
[VAT19]	E. Vlachos, G. C. Alexandropoulos, and J. Thompson, "Wideband MIMO channel estimation for hybrid beamforming millimeter wave systems via random spatial sampling," IEEE J. Sel. Topics Signal Process., vol. 13, no. 5, pp. 1136–1150, Sep. 2019.
[VCA+18]	Y. Vahabzadeh, N. Chamanara, K. Achouri and C. Caloz, "Computation Analysis of Metasurfaces", IEEE Journal on Multiscale and Multiphysics Computational Techniques, vol. 3, pp. 37-49, 2018.
[VGT14]	F. W. Vook, A. Ghosh and T. A. Thomas "MIMO and Beamforming Solutions for 5G Technology," IEEE MTT-S IMS, pp. 1-4, June 2014.
[W+11]	M. Wang et al., "Evaluation and optimization of the specific absorption rate for multiantenna systems," IEEE Trans Electromagn. Compat., vol. 53, no. 3, pp. 628–637, Aug. 2011.
[W+20]	R. Wang et al., "Enabling Super-Resolution Parameter Estimation for mm-Wave Channel Sounding," IEEE Tran. on Wireless Comm., Vol. 19, no. 5, May 2020.
[WK14]	Z. Wen and H. Kong, "mmWave MIMO channel sounding for 5G," 1st International Conference on 5G for Ubiquitous Connectivity, Nov. 2014.
[WZ19]	Q. Wu and R. Zhang, "Joint active and passive beamforming optimization for intelligent reflecting surface assisted SWIPT under QoS constraints," arXiv:1910.06220, 2019.
[WZ20]	Q. Wu and R. Zhang, "Weighted sum power maximization for intelligent reflecting surface aided SWIPT," IEEE Wireless Commun. Lett., vol. 9, no. 5, pp. 586–590, May 2020.
[XZY+19]	Xu, K. Zhao, Z. Ying, D. Sjöberg, W. He and S. He, "Analysis of Impacts of Expected RF EMF Exposure Restrictions on Peak EIRP of 5G User Equipment at 28 GHz and 39 GHz Bands," IEEE Access, vol. 7, pp. 20996-21005, February 2019.

[YIP22]	Y. Yu, R. Ibrahim, D.-T. Phan Huy “EMF-Aware MU-MIMO Beamforming in RIS-Aided Cellular Networks,” submitted to IEEE Globecom 2022.
[YXA+21-1]	J. Xu, L. You, G. C. Alexandropoulos, J. Wang, W. Wang, and X. Q. Gao, “Dynamic metasurface antennas for energy efficient uplink massive MIMO communications,” in Proc. IEEE GLOBECOM, Madrid, Spain, 2021, pp. 1–6.
[YXA+21-2]	L. You, J. Xu, G. C. Alexandropoulos, J. Wang, W. Wang, and X. Gao, "Energy efficiency maximization of massive MIMO communications with dynamic metasurface antennas," IEEE Trans. Wireless Commun., under revision, 2021.
[Z+21]	A. Zappone et al., “Overhead-aware design of reconfigurable intelligent surfaces in smart radio environments,” IEEE Trans. Wireless Commun., vol. 20, no. 1, pp. 126–141, Jan. 2021.
[ZHL14]	H. Zhou, L. M. Huie, and L. Lai, “Secret key generation in the two-way relay channel with active attackers,” IEEE Trans. Inf. Forensics Security, vol. 9, no. 3, pp. 476–488, Mar. 2014.
[ZR22]	A. Zappone, M. di Renzo “Energy Efficiency Optimization of Reconfigurable Intelligent Surfaces with Electromagnetic Field Exposure Constraints”, submitted to Signal Processing Letters 2022, available at: https://arxiv.org/abs/2104.06283.
D2.3	RISE-6G Deliverable D2.3 “Reference system, scenarios and use cases analysis: final results”, Feb. 2022.
D2.4	RISE-6G Deliverable D2.4 “Metrics and KPIs for RISE wireless systems analysis: final results”, Feb. 2022.
D6.1	RISE-6G Deliverable D6.1 "Network architectures & deployment strategies with RIS for enhanced EE, EMFEU, and SSE (Intermediary Specifications)" May 2022.